Williams-Jones, A., and Vasyukova, O., 2022,
Constraints on the genesis of cobalt deposits: part I. Theoretical considerations: Economic Geology, v. 117, p. 513-528.

CONSTRAINTS ON THE GENESIS OF COBALT DEPOSITS: PART I, THEORETICAL CONSIDERATIONS

A.E. Williams-Jones and O.V. Vasyukova

Department of Earth and Planetary Sciences, McGill University, 3450 University Street Montréal, Québec, Canada, H3A 0E8

Abstract

Cobalt is in high demand because of the key role that cobalt-lithium-ion batteries are playing in addressing the issue of global warming, particularly in facilitating the transition from the internal combustion engine to electrically-driven vehicles. Here, we review the properties of cobalt and the history of its discovery, briefly describe its mineralogy and explore the processes that concentrate it to potentially exploitable levels. Economic cobalt deposits owe their origin to the compatible nature of Co^{2+}, its concentration in the mantle in olivine, and its release, after high degrees of partial melting, to komatiitic and to a lesser extent, basaltic magmas. Primary magmatic deposits, in which Co is subordinate to Ni, develop through the separation of immiscible sulfide liquids from mafic and ultramafic magmas, as a result of the very strong preference of these metals for the sulfide liquid and its crystallization, which culminates with exsolution of the Fe-Ni-Co sulfide mineral, pentlandite (from monosulfide solid solution). We evaluate the factors that concentrate cobalt to economic levels by these processes. Cobalt is also concentrated by aqueous fluids, either at ambient temperature in laterites developed over ultramafic rocks or hydrothermally in sediment-hosted copper deposits and in cobalt-rich vein deposits, where it crystallizes mainly as sulfide and arsenic-bearing minerals, respectively. Using the available thermodynamic data for aqueous Co species, we evaluate cobalt speciation as a function of temperature and show that, whereas at ambient temperature, it is transported as the simple ion (Co^{2+}), at elevated temperature, it is most mobile as chloride species. Based on thermodynamic data compiled from a variety of sources, we evaluate stability relationships among some of the principal cobalt sulfide and oxide minerals as a function of temperature, pH, fO_2, and αH_2S, and, in conjunction with the aqueous speciation data, determine their solubility. This information is used, in turn, to predict the physicochemical conditions most favorable for cobalt transport and ore formation by hydrothermal fluids. As thermodynamic data are not available for the cobalt arsenide and sulfarsenide minerals that form the vein-type ore deposits, we use chemographic analysis to evaluate their stability relationships

qualitatively and predict the physicochemical controls of ore formation. The data and interpretations of processes presented in this paper provide the theoretical basis for a companion paper (Vasyukova and Williams-Jones, 2021), in which we develop plausible models for the genesis of the principal cobalt deposit types.

Introduction

A variety of technological advances, notably the development of cobalt-lithium-ion batteries, have created a high demand for cobalt that is expected to continue as electrically-driven vehicles replace vehicles driven by internal combustion engines. Presently, Co-Li-ion batteries make up 49 % of the demand for Co (Fig. 1a) and this demand is predicted to reach 80 % in 2030 (Dias et al., 2018; Fig. 1b). The next most important application of cobalt is in the manufacture of super-alloys (18 % of consumption, Fig. 1a) with very high thermal and corrosion resistance for use in the aerospace and automotive industries. Other uses of cobalt include the production of catalysts, pigments, Co-Ni-Fe magnets (5, 6 and 3 % of consumption, respectively, Fig. 1a), and the application of the radio-isotopes, ^{60}Co and ^{57}Co, in medicine.

The increased demand has created a pressing need to find new resources of cobalt. Over 50 % of the World's current supply of cobalt (Fig. 2) is from the Democratic Republic of Congo (DRC), a country that has been in a state of civil war for at least 20 years. Most of the remaining supply is as a by-product of the mining of Ni in magmatic sulfide (23 %) and laterite deposits (15 %). The deposits in the DRC are hosted by a belt of metasedimentary rocks that straddles the DRC/Zambia border. They are exploited primarily for their copper content and have Cu:Co ratios that average 13:1 and reach 3:1 (Cailteux et al., 2005); cobalt grades range from 1.12 to 0.06 wt. % (Slack et al., 2017). Magmatic Ni-Co deposits develop as a result of sulfide-silicate immiscibility in mafic and ultramafic igneous magmas (Naldrett, 2004a) and have Ni:Co ratios ranging from ~15:1 in ultramafic magma-related deposits to ~ 30:1 in mafic magma-related deposits (Barnes and Lightfoot, 2005, Slack et al., 2017). The average Co grade is 0.07 wt. % and ranges between 0.01 and 0.6 wt.% Co, with the higher grades being for deposits associated with ultramafic rocks (Slack et al., 2017). The next most important sources of cobalt are Ni-Co laterites, which are developed over olivine-rich ultramafic rocks, such as dunite and lherzolite (Freyssinet et al., 2005). These deposits typically contain Ni and Co in the ratio 20:1 (Berger et al., 2011), and have Co grades between 0.03 and 0.22 wt. % or 0.08 wt.% on average (Slack et al., 2017). The remaining 2 %

comes from hydrothermal vein type deposits associated with serpentinites (Fig. 2), primarily from the Bou Azzer district in Morocco, where they are developed at the contacts between the serpentinites and quartz diorite intrusions or felsic volcanic rocks (En-Naciri et al., 1997, Dolansky, 2007, Bouabdellah et al., 2016). These deposits are the only primary producers of cobalt and contain this metal in a concentration of ~1 wt. % (Bouabdellah et al., 2016).

In this paper, we examine the chemical characteristics of cobalt, review its mineralogy and incorporation in common rock-forming minerals and discuss its behavior in magmas and aqueous fluids. Using this background, we then proceed to a discussion of the processes that concentrate cobalt to economic levels in nature. This information forms the basis for a companion paper (Vasyukova and Williams-Jones, 2021), in which we use the information presented here to discuss genetic models for the principal types of cobalt deposits mentioned above.

Discovery of cobalt

Although cobalt has been known since the Bronze age in Egypt and Persia, where it was used as a dye in glass and ceramics (a large glass bead doped with cobalt to produce its blue color was found in the tomb of the pharaoh, Tutankhamun, 1341 BCE to 1323 BCE), it was only identified as a new element in the 1700s. Indeed, it was the first metal to be discovered in the modern era. Cobalt was shown to be a new metal by the Swedish chemist, Georg Brandt, who, in 1735, separated it by roasting Co-Ni arsenide ores. This produced a black powder, which he reacted with charcoal to produce a pink metal that he named cobalt. The name comes from the German word, 'kobold', for 'goblin' or 'evil sprite', because of the arsenic contained in the ores, which led to the premature death of miners. Brandt also discovered that cobalt can be alloyed with other metals, like iron, tin, copper, gold, and antimony.

It was not until the 1800s that cobalt was recognized as an element. The first step in this recognition was the observation by John Dalton, an English schoolteacher, chemist, physicist, and meteorologist, that substances could be reduced to single entities (atoms), which could be ordered according to their atomic weight. Realizing that it would not be possible to determine atomic weights absolutely, he normalized them to the atomic weight of hydrogen, which he arbitrarily assigned a value of 1. Dalton produced a table of atomic weights for thirty elements but in the case of cobalt could only conclude that it must have an atomic weight between 50 and 60 (Dalton,

1808). It was left to Jöns Berzelius, a Swedish chemist, to produce the first comprehensive list of atomic weights (Berzelius, 1818). He determined the atomic weight of cobalt to be 59.03, which is remarkably close to the currently accepted atomic weight of 58.93. In 1869, Dmitri Mendeleev incorporated cobalt in the periodic table and assigned it the atomic number 27.

Properties of cobalt

Cobalt is a transition metal in Group 9 of the Periodic table with the electronic configuration [Ar] 3d7 4s2. In nature, it occurs almost exclusively as ^{59}Co (four radioisotopes of cobalt have been identified, with half-lives ranging from 77 days to 5.27 years) and, like iron, is a ferromagnetic metal. It has a Curie temperature of 1,115 °C, a melting temperature of 1,495°C, a boiling point of 2,927 °C and a density is 8.9 g/cm^3. Cobalt has two main oxidation states, namely 2+ and 3+. In minerals, it occurs dominantly in octahedral coordination with an ionic radius that varies between 0.65 Å (low spin) and 0.75 Å (high spin) for Co^{2+} and 0.55 Å (low spin) and 0.61 Å (high spin) for Co^{3+}. In minerals, it occurs dominantly in the high spin state. Cobalt has an electronegativity of 1.88 and the second and third ionization energies are 1,648 and 3,232 kJ/mol, respectively. The latter are significantly larger than the corresponding energies for Fe (1,561 and 2,957 kJ/mol), consistent with the observation that Co is significantly more resistant to oxidation than Fe, but lower than those of nickel (1,753 and 3,395 kJ/mol).

Mineralogy

Cobalt has a strong affinity for reduced sulfur and arsenic, and occurs most commonly in nature as sulfides, sulfarsenides and arsenides. It is also commonly associated with nickel and, in some cases, Cu, in these phases. The principal hypogene ore minerals for cobalt are carrollite ($Cu(Co,Ni)_2S_4$), cobaltpentlandite ($(Co,Ni,Fe)_9S_8$), cattierite (CoS_2), siegenite ($CoNi_2S_4$), linnaeite ($Co^{2+}Co^{3+}{}_2S_4$), cobaltite (CoAsS), alloclasite ($Co_{1-x}Fe_x$)AsS, skutterudite ($CoAs_3$) and safflorite ($(Co,Ni,Fe)As_2$) (Table 1). Cobalt also occurs as supergene minerals, either erythrite ($Co_3(AsO_4)\cdot 2.8H_2O$), in the case arsenide or sulfarsenide precursors, or the hydrous oxides, heterogenite (CoOOH) and asbolane ($(Ni,Co)_{2-x}Mn^{4+}(O,OH)_4\cdot nH_2O$), which are also the principal cobalt ore minerals in laterites (Table 1). Heterogenite is the main mineral exploited in the supergene ores of the sediment hosted Cu-Co deposits of the DRC.

Sources of Cobalt

A prerequisite for understanding the concentration of any metal to exploitable levels is knowledge of the principal reservoirs of the metal. By far the greatest reservoir for cobalt is the mantle, in which its average content is 102 ppm (Palme and O'Neill, 2014). In contrast, the continental crust only contains 27 ppm Co and the concentration of Co decreases from 38 ppm in the lower continental crust to 17 ppm in the upper continental crust (Rudnick and Gao, 2014). The oceanic crust has a Co content of 44 ppm (White and Klein, 2014), which is intermediate between that of the mantle and the upper continental crust.

Processes concentrating cobalt

Magmatic processes

As noted earlier, over 20 % of cobalt production comes from the mining of magmatic Ni-Cu sulfide deposits. Here, we discuss the processes that are responsible for the concentration of cobalt in magmas. These are partial melting, fractional crystallization and liquid immiscibility. From the preceding discussion of sources, it is evident that Co reaches its highest concentration in peridotite and decreases to roughly half this concentration in gabbro; in granite the concentration is only 5 % of that in peridotite. It, therefore, follows that the magmas that are important for concentrating cobalt are ultramafic to mafic in composition and are the products of high degrees of partial melting of the mantle. Below, we evaluate the effects of fractional crystallization and liquid immiscibility on the concentration of Co in mafic and ultramafic rocks.

Fractional crystallization

Magmas commonly evolve by fractional crystallization, during which trace elements of interest are either compatible (they partition preferentially into the early formed minerals) or incompatible (they concentrate in the residual liquid). Consequently, fractional crystallization plays an essential role in determining the fate of trace metals, i.e., whether they are enriched or depleted in the magma. Because cobalt has an ionic radius of 0.75 Å (high spin), i.e., intermediate between those of Mg (0.72 Å) and Fe (0.78 Å), it tends to concentrate preferentially in ferromagnesian minerals, such as olivine and pyroxene. Thus, cobalt is compatible during the crystallization of ultramafic and mafic magmas.

We employed the Co mineral-melt partitioning equations for olivine, orthopyroxene and clinopyroxene reported by Bedard (2005, 2007, 2014) to evaluate the effect of fractional

crystallization on the concentration of cobalt in magmas. The partition coefficients for these minerals vary systematically with a number of parameters, e.g., the Al_2O_3, SiO_2 and MgO contents of the magma and temperature. The strongest correlation, however, is with the MgO content of the magma, which in logarithmic form varies inversely with the logarithm of the partition coefficient for all three minerals. Therefore, we evaluated cobalt mineral-melt partitioning using the equations for MgO (Fig. 3). The partition coefficients for the three minerals are all > 1, if the MgO content of the corresponding magma is < 37 wt.%, < 13 wt.% and < 9 wt.% for olivine, orthopyroxene and clinopyroxene, respectively. Thus, cobalt partitions preferentially into olivine but, in the absence of olivine, will partition into the melt rather than into orthopyroxene or clinopyroxene, if the MgO content of the magma is > 13 or > 9 wt.%, respectively. The partition coefficient equations referred to above also predict, in the case of co-crystallization, that cobalt prefers olivine over orthopyroxene and orthopyroxene over clinopyroxene for magmas containing up to 24 wt.% MgO, i.e., most mafic and ultramafic magmas. We believe that this is because the ionic radius of Co is significantly larger than that of Mg (0.75 vs 0.72 Å), which makes it difficult for Co to substitute into a Mg-rich ferro-magnesian mineral (the presence of Fe with an ionic radius 0.78 Å facilitates this substitution), and for the same temperature and pressure the Fe/Mg ratio of the mineral decreases in the order olivine>orthopyroxene>clinopyroxene.

Using the partition coefficient data reported above, we modelled the fractional crystallization of komatiitic and basaltic magmas to determine the extent to which crystallization of ferro-magnesian minerals, particularly olivine, affects the Co content of the magma. This was done using the program Pele (Boudreau, 1999). For the komatiitic magma, we used the composition of a high Mg flow-top komatiite from Tisdale Township, Ontario, Canada, reported in Sproule et al. (2002). This sample was chosen because it represents a chilled margin and has a composition similar to that of the magma prior to crystallization (Table 2). The Co content of the komatiite is 104 ppm, which is very similar to that of the average mantle (see above). In modelling the crystallization, we assumed that the magma cooled from a temperature of 1600 ºC to 1150 ºC in 50 ºC steps at 100 bar (the lowest pressure permitted by the program), the pressure reflecting the fact that cobalt deposits forming from komatiitic magmas are hosted by lavas. The Co olivine-melt partition coefficients were re-calculated for the MgO content of the magma at each step (pyroxene does not crystallize at the above conditions). This modelling demonstrated that fractional crystallization depletes the magma in Co but that this depletion is relatively modest, i.e., after ~50 %

crystallisation, the concentration of Co in the residual magma was ~65 ppm (Fig 4a; Table 3). It also showed that the concentration of Co in the resulting olivine cumulates reaches 145 ppm (the enrichment factor, i.e., the ratio of the final concentration to the initial concentration is, thus, 1.4), which is insufficient to make an ore, but could be important in providing the metal source for hydrothermal and laterite Co deposits.

The fractional crystallization of basaltic magma was modelled using the composition of aphyric Siberian flood basalts in the Norilsk district, Russia (Krivolutskaya et al., 2018), which are cogenetic with the magmas that produced the giant Norilsk magmatic sulfide deposits (Naldrett, 2004b)); the average Co content for the Siberian flood basalts in the Norilsk district (44 ppm) was taken from Lightfoot et al. (1993). The modelling was conducted for a magma cooling from 1200 ºC to 900 ºC in 50 ºC steps (the composition of this magma is reported in Table 2) and the pressure was assumed to be 500 bars, which corresponds to the emplacement depth of 1-2 km for the Norilsk intrusions (Sluzhenikin et al., 2014). The modelling software and partition coefficient equations were the same as those described above. Fractional crystallization of the magma reduced the Co content of the residual liquid progressively from 44 ppm, initially, to a concentration of 37 ppm after 20 % crystallisation and 3 ppm after 70% crystallisation (Fig. 4b; Table 3). Our modelling showed that the concentration of Co in the crystal cumulate (olivine and clinopyroxene) reached a maximum of 227 ppm after ~ 20% crystallization, which is considerably higher than the maximum of 145 ppm reached in the olivine cumulate formed during crystallization of the komatiitic magma, and corresponds to an enrichment factor of 5.2. Although, separation of a crystal cumulate of olivine and clinopyroxene at this stage of fractional crystallisation would be insufficient to form an ore deposit, it could provide an excellent source of Co for hydrothermal and laterite Co mineralization. With further fractional crystallization, the Co content of the cumulate gradually decreased to 127 ppm after 80% crystallization.

Liquid immiscibility

Magmatic sulfide deposits, as mentioned earlier, form as a result of sulfide-silicate immiscibility. Assuming an average mantle S concentration of ~200 ppm (Palme and O'Neil, 2014), 50 % partial melting, and a mantle-melt partition coefficient for sulfur of zero, the magma would contain ~ 400 ppm S. This would also be close to the sulfur concentration at sulfide saturation because of the likely coexistence of the magma with residual sulfides in the mantle (Mavrogenes and O'Neill,

1999). On extrusion or emplacement as a shallow intrusion, however, this magma, would be highly undersaturated in respect to sulfur. This is because, as shown experimentally by (Mavrogenes and O'Neill, 1999), the solubility of sulfur increases sharply with decreasing pressure in mafic (basaltic) and ultramafic (picritic) magmas. Indeed, for the mafic (synthetic basalt) composition considered in their experiments, the sulfur content at sulfide saturation is predicted to rise from 345 ppm at 1,400 °C and 60 kbar (mantle conditions) to 1,075 ppm at 1,200 °C and 1 bar. An external source of sulfur is therefore required to explain the genesis Co-bearing magmatic sulfide ore deposits.

The solubility of sulfur in magmas depends on a number of factors including temperature, pressure, composition and fO_2. The last of these is particularly important because the solubility of sulfur in mafic to ultramafic magmas increases sharply at fO_2 values ~1-2 log units above the fayalite-magnetite-quartz (FMQ) buffer (over an order of magnitude between FMQ+1 and FMQ+2) due to the change from sulfide (S^{2-}) to sulfite (S^{4+}) and sulfate (S^{6+}) as the dominant dissolved sulfur species (Carroll and Rutherford, 1988, Jugo et al., 2005). As a result, these magmas are able to dissolve high concentrations of sulfur at elevated fO_2 that can be employed in sequestering Co during the exsolution of a sulfide liquid. The most common sulfur source is sulfidic black shale or its metamorphosed equivalent, although in some cases, notably the Noril'sk-Talnak deposits, Russia, as discussed in Vasyukova and Williams-Jones (2021), the source of sulfur was evaporite (anhydrite); dissolution of the anhydrite also facilitates sulfur uptake by imposing a high fO_2 on the magma.

On the separation of a sulfide liquid, metals like Ni, Cu and Co partition preferentially into this liquid. Several experimental studies have investigated the partitioning of Co between sulfide and mafic-ultramafic silicate melts, e.g., Gaetani and Grove (1997), Kiseeva and Wood (2013) and Li and Audétat (2015). Sulfide-silicate partition coefficients for Co have also been reported for coexisting basaltic glass and sulfide globules from mid-ocean ridge basalts (Peach et al., 1990, Patten et al., 2013). With the exception of Gaetani and Grove (1997), the experimental studies were all conducted with basalt (and more felsic starting compositions, in the case of Li and Audétat, 2015) and at a pressure of 15 kbar (Li and Audétat, 2015, also conducted experiments at 5 and 8 kbar). The study of Gaetani and Grove (1997) involved a komatiitic liquid and a pressure of 1 bar. These studies all show that the partition coefficient is dependent on fS_2, fO_2 and the

238 FeO_{tot} concentration of the silicate magma, but that any two of these parameters constrain the third.
239 The study of Li and Audétat (2015) demonstrated that D_{Co} is also dependent on temperature. In
240 addition, they concluded that, within the pressure range of their experiments (5 - 15 kbar), D_{Co} is
241 independent of pressure and, except for FeO_{tot}, is independent of the composition of the magma.
242 The other experimental studies referred to above were conducted at a single temperature (1350 °C
243 in the case of Gaetani and Grove, 1997; and 1400 °C in the case of Kiseeva and Wood, 2013).

244 Li and Audétat (2015) developed an equation, based on their experimental data, that makes it
245 possible to calculate $\log D_{Co}$ at any temperature, if fO_2 and FeO_{tot} are known (see their equation
246 5), thereby providing a basis for comparing the results of the different studies. Using this equation,
247 we calculated Co sulfide-silicate partition coefficients (D_{Co}) for the run products in the other
248 experimental studies and the two studies of natural samples from the FeO_{tot} contents of the glasses
249 and fO_2. Except for Gaetani and Grove (1997), who reported fO_2 values, assumptions had to be
250 made about the fO_2 conditions. The experiments of Kiseeva and Wood (2013) were all conducted
251 in graphite crucibles, allowing us to assume that fO_2 was controlled by the graphite-CO_2 buffer.
252 In the case of the two mid-ocean ridge studies (Peach et al. (1990) and Patten et al. (2013)), it was
253 also necessary to assume a temperature, which we took to be 1200 °C; oxygen fugacity was
254 assumed to have been buffered by FMQ following Cottrell and Kelley (2011). From Figure 5, it is
255 evident that the partition coefficients for cobalt reported by the various studies are in very good
256 agreement and that Equation 5 of Li and Audétat (2015) can be used reliably to predict D_{Co} values
257 for both basaltic and komatiitic magmas.

258 As a first step in evaluating the concentration of cobalt in ore-forming sulfide liquids separating
259 from basaltic and komatiitic liquids, we used Equation 5 of Li and Audétat (2015) to determine a
260 D_{Co} value for the komatiites of the Kambalda magmatic sulfide district in Australia. Consistent,
261 with our earlier observation that mantle-derived mafic and ultramafic magmas are undersaturated
262 in respect to a sulfide liquid prior to eruption, these magmas are interpreted to have saturated with
263 sulfide liquid as a result of assimilation of graphite-bearing sulfidic sediments (Huppert et al.,
264 1984). We, therefore, assumed that, on saturating with a sulfide liquid, the fO_2 of the parental
265 magma was equivalent to that of the graphite-CO_2 buffer (calculated using equation A1a of
266 Holloway et al., 1992). Using this fO_2, a temperature of 1400 °C and the average FeO_{tot} content
267 of Kambalda komatiites (10.1 wt.%) reported by Arndt and Jenner (1986), we obtained a value of

D_{Co} of 83; the komatiite used to model the effect of fractional crystallization, which has a higher FeO_{tot} content (11.1 wt%), yielded a slightly lower value of D_{Co} (74). To represent a mafic magma, we used the Siberian flood basalts, which, as mentioned above, are cogenetic with the magmas that produced the giant Noril'sk-Talnak magmatic sulfide deposits, Russia, and, thus, are an appropriate proxy for these magmas. As both the Noril'sk-Talnak magmas and the Siberian flood basalts interacted with coal measures during their emplacement (Naldrett, 2004b, Elkins-Tanton et al., 2020), we assumed a value of fO_2 equivalent to that of the graphite-CO_2 buffer (calculated using equation A1a of Holloway et al., 1992, for a pressure of 500 bars, see above, and CO2 fugacity coefficient data from Duan et al., 1992). Based on this value of fO_2, a temperature of 1200 °C, and the average FeO_{tot} content of the Siberian traps in the Noril'sk area (10.1 wt.%), from Krivolutskaya et al. (2018), the value of D_{Co} was calculated to be 68.

The concentration of Co in a sulfide liquid depends not only on the partition coefficient but also on the initial Co concentration of the silicate melt and the silicate-sulfide mass ratio. These parameters can be used to calculate the concentration of Co in this liquid from the relationship

$$Y_i^{sul} = (X_i^{sil} \cdot D \cdot (1+R))/(R+D) \quad (1)$$

or

$$Y_i^{sul} = X_i^{sil} \cdot (D-((D-1)*e^{-(1/D*N)})) \quad (2)$$

where Y_i^{sul} is the final concentration of element i in the sulfide liquid, X_i^{sil} is the initial concentration in the silicate liquid, D is the sulfide-silicate melt partition coefficient and R and N are the silicate-sulfide mass ratios (Naldrett, 2004c). The parameters R and N indicate the degree of sulfide super-saturation of the magma, with a small value reflecting a very high degree of supersaturation and a large value relatively limited supersaturation. Equation 1 containing the term "R" is used, if it is assumed that the sulfide liquid equilibrated with a single batch of magma that was then removed (i.e., a closed system). If, however, the sulfide liquid is assumed to have reacted continuously with new batches of fresh magma (i.e., an open system), Equation 2 containing the term "N" is used. We have employed the above equations to predict the Co concentration of sulfide liquids separating from komatiitic and basaltic magmas for a variety of R and N values (Table 4). The initial Co concentrations in the silicate liquid were assumed to be 104 and 44 ppm,

296 respectively, which are the values that we used in our modeling of the effect of fractional
297 crystallisation on Co content (see above). The partition coefficients were taken to be 83 and 68,
298 respectively (also see above). Our calculations show that for komatiitic magmas in closed systems,
299 the Co concentration in the sulfide liquid increases from 206 ppm for an R factor of 1 to 4,764 and
300 7,978 ppm for R factors of 100 and 1,000, respectively. A further increase in the R factor to 10,000
301 only raises the Co concentration to 8,562 ppm (Table 4). If the sulfide liquid is continuously
302 exposed to fresh komatiitic magma, the concentration of Co in the sulfide melt increases more
303 sharply to values of 6,076 and 8,632 ppm for N values of 100 and 1,000, respectively, and does
304 not increase further (Table 4). The Co concentrations of sulfide liquids separating from basaltic
305 magmas are more modest. In closed systems, they rise from a Co concentration of 87 ppm for a R
306 factor of 1 to 1,799 and 2,804 ppm for R factors of 100 and 1,000, respectively; raising the R value
307 to 10,000 leads only a small (168 ppm) additional increase in Co concentration (Table 4). As in
308 the case of komatiites, if the system is open, the Co concentration increases more sharply, i.e.,
309 from 87 ppm for a N value of 1 to 2,315 and 2,992 ppm for N values of 100 and 1000, respectively.
310 To summarize, in both closed and open magmatic systems, sulfide-silicate liquid immiscibility
311 provides an extremely effective means of concentrating cobalt to potentially economic levels, if
312 the dense sulfide liquid is able to extract Co efficiently from the silicate liquid (by equilibrating
313 with it) and then is accumulated by gravity settling (the enrichment factors for komatiite and basalt
314 are potentially ~46(58) and ~41(53), respectively for a R(N) factor of 100).

315 Unlike Cu, which may concentrate further during cooling of the sulfide liquid, because of the
316 fractional crystallization of monosulfide solid solution and the strong preference of Cu for the
317 residual liquid, Co partitions almost equally between the two phases and does not undergo
318 additional concentration (Li and Audétat, 2015). Although, further cooling eventually leads to the
319 exsolution of pentlandite (below 850 ºC; Naldrett, 2004c), this occurs after complete
320 crystallization of the sulfide liquid (above 1000 ºC because the composition of the latter is very
321 close to that of FeS; Naldrett, 2004c), and, consequently, has no effect on the composition of the
322 ore and the concentration of Co.

323 In addition to undergoing sulfide-silicate liquid immiscibility, mafic magmas may also undergo
324 silicate-silicate immiscibility, provided that they are enriched in alkalis (Roedder and Weiblen,
325 1970, Philpotts, 1972, Eby, 1979). Such immiscibility is characterized by the separation of a felsic

melt from a mafic melt, as described by Philpotts (1972) for mafic dykes and sills of the Monteregian Hills, Canada. The felsic melts (ocelli) are enriched in silica, alumina and the alkalis, whereas the host dyke/sill is enriched in calcium, magnesium and, particularly, iron, but depleted in silica (Philpotts, 1972). These intrusions contain small concentrations of cobalt (10-30 ppm), but more importantly, show evidence of preferential partitioning of the cobalt into the residual silica-poor but Fe-rich magma; the partition coefficient is ~ 3 (Eby, 1979). In addition to the data for natural systems, the partitioning of cobalt between alkaline mafic and felsic melts has been investigated experimentally. Lester et al. (2013) showed that the partition coefficient for Co between mafic (Fe-rich) and felsic (Si-rich) magmas varies between 5 and 17, depending on the composition of the magma prior to separation. They also found that the partitioning of cobalt into the mafic melt is strongly favored by high concentrations of sulfur, phosphorous and fluorine. Thus, in principle, silicate-silicate liquid immiscibility in alkali-rich magmatic systems could fractionate cobalt efficiently, particularly if the proportion of felsic magma is large relative to that of the conjugate mafic magma (see earlier discussion of the role of the R/N parameter in cobalt concentration). It is important to note, however, that alkaline magmas result from low degrees of partial melting of the mantle, whereas Co-rich magmas form only after high degrees of partial melting, due to the preference of Co for the ferromagnesian minerals like olivine that dominate the mantle. Consequently, even if mafic-felsic liquid immiscibility strongly promotes the concentration of Co, the extremely low initial Co content of the primary alkaline magma precludes the formation of economic Co deposits by this process.

The only other magmas that exsolve from silicate magmas in appreciable volumes are carbonate magmas (Lebas, 1981, Kjarsgaard and Hamilton, 1988, Weidendorfer et al., 2016). Although a number of studies have investigated this phenomenon experimentally (Veksler et al., 1998, Brooker and Kjarsgaard, 2011, Veksler et al., 2012, Martin et al., 2013), to our knowledge, only Martin et al. (2013) have reported data for the partitioning of cobalt between the two magmas. Their partition coefficients range between ~3 and ~0.2 depending on the pressure and whether the system was anhydrous or hydrous. Given the small size of the partition coefficient and the probable low concentration of cobalt in the parental silicate magma, due to the high degree of compatibility of cobalt (this magma is the product of a small degree of partial melting of a carbonated mantle), it is also unlikely that silicate-carbonate immiscibility would contribute to the formation of economic cobalt deposits.

The magmatic-hydrothermal transition

In addition to the magmatic processes described above, the exsolution of an aqueous phase can also play a major role in the transport of metals, including Co. Thus, for example, the ores of porphyry, IOCG (Iron-Oxide-Copper-Gold) and skarn deposits are the products of such fluids and, in some cases, these ores can contain significant concentrations of cobalt (Wang and Williams, 2001, Sillitoe, 2003, Soloviev et al., 2013). Here, we discuss the magmatic-hydrothermal transition in the context of cobalt ore formation.

The solubility of water in all common silicate magmas reaches in excess of 5 wt.% (Webster et al., 1999, Mitchell et al., 2017). Therefore, as unaltered igneous rocks typically contain less than 1 wt.% H_2O, most magmas should exsolve substantial quantities of hydrothermal fluid. Significantly, however, basaltic and komatiitic magmas rarely give rise to magmatic-hydrothermal ore deposits. The reason for this is that in all tectonic environments, except subduction zones, such magmas are relatively dry (0.1 to 0.5 wt.% H_2O; Johnson et al., 1994), and, thus, will only exsolve an aqueous phase at a very advanced stage of crystallisation. As cobalt is a compatible element, crystallisation of minerals, like olivine and pyroxene, would have removed most of the cobalt leaving little to partition into the aqueous phase. Basaltic magmas produced in subduction zones, however, will be relatively enriched in Co at the time of aqueous phase exsolution, which is early because of their high water content (in some cases in excess of 6 wt.%; Sisson and Layne, 1993).

To further evaluate the role of magmatic hydrothermal fluids in concentrating Co, information is required on its partitioning between aqueous fluids and magmas. In the absence of such information, we have used Fe as a proxy for Co (they have very similar properties), and extracted a partition coefficient for Fe between rhyolite and a supercritical fluid from the data of Simon et al. (2004). These authors investigated the solubility of magnetite in a system containing rhyolite and fluid at 800 ºC and 1 kbar, and reported the Fe contents of the two phases; the data yield a fluid-melt partition coefficient of 0.2. Assuming a similar partition coefficient for cobalt, it follows that the concentration of Co in fluids exsolving from rhyolitic magmas is likely to be very low. As mafic and, particularly, ultramafic magmas are much less polymerised than rhyolitic magmas, they will more easily accommodate divalent cations like Fe^{2+} and Co^{2+}, the fluid-melt partition coefficients for these magmas will be << 0.2. Based on the average Co contents of basalt and komatiite (44 and 104 ppm, respectively), the corresponding Co concentrations in the fluid would

be <<9 and <<21 ppm, respectively. Thus, even in a case of hydrous magmas of Alaskan-type ultramafic intrusions (considered to form in subduction zones), the concentration of Co by the exsolving hydrothermal fluids is likely to be insignificant.

A possible means by which cobalt could be concentrated to exploitable levels by magmatic-hydrothermal fluids is through the prior fractionation of cobalt into a sulfide liquid and the dissolution of this liquid and/or resulting solids by an aqueous fluid exsolving from the coexisting silicate melt, as proposed for Cu in porphyry systems by Keith et al. (1997), Halter et al. (2002) and Nadeau et al. (2010). According to this model, the resident felsic magma is not the ultimate source of the metals. Instead, the metals are introduced by small volumes of sulfide-saturated mafic magmas that are injected into the crystallising felsic magma. This model for cobalt is supported by the observation of Nadeau et al. (2010) that the Co/Ni ratio in fumarolic gases of an arc volcano (Merapi) is very similar to that of sulfide melt inclusions in mafic tephra from the same volcano. As Co partitions strongly into sulfide melts (see above), and Co contents in the latter can reach in excess of 2,000 ppm (Vasyukova and Williams-Jones, 2021), dissolution of these melts by a magmatic-hydrothermal fluid could lead to substantially higher Co concentrations in the aqueous phase (perhaps an order of magnitude higher; see below) than predicted by silicate melt-fluid partitioning. In summary, hydrothermal fluids exsolving from silicate magmas are unlikely to attain ore-forming concentrations of Co unless they dissolve a coexisting sulfide magma.

Aqueous processes

Transport

At ambient temperature, the simple ion, Co^{2+}, is likely to play an important role in cobalt mineral dissolution because of the high dielectric constant of water (e.g., Eugster, 1986), which ensures the development of strong solvation shells. At higher temperature, however, cobalt mineral dissolution will be dominated by the formation of complex species, provided that appropriate ligands are available for complexation. As Co^{2+} is a borderline acid, it is predicted to form its strongest aqueous complexes with borderline bases (Pearson, 1963, Williams-Jones and Migdisov, 2014). The only borderline base of any significance is Cl^-, which is the principal ligand in most natural waters. Cobalt could, in principle, also form stable complexes with other ligands that are present in significant concentrations in aqueous fluids, e.g., bisulfide (soft) and hydroxide (hard) ions.

As expected, the available thermodynamic data for 25 ºC show that the simple ion makes up a significant proportion of the dissolved cobalt in most aqueous fluids. They also show, however, that even at this low temperature, cobalt forms stable complexes with chloride ions. There have been relatively few studies of cobalt chloride complexation at ambient temperature, and there is considerable disagreement over the stability of the different complexes. The formation constants reported in these studies were reviewed by Pan and Susak (1989), who also reported formation constants for chloride complexes based on the results of their own experiments for temperatures from 25 to 90 ºC. Based on the formation constants recommended by Pan and Susak (1989), $CoCl^+$ dominates cobalt mineral solubility at 25 ºC for a chlorinity between ~0.5 and ~2.5, whereas $CoCl_2^o$ and $CoCl_4^{2-}$ are dominant at higher chlorinity. Several studies have reported formation constants for $CoHS^+$ and $Co(HS)_2^o$ at 25 ºC, and, as in the case of the chloride complexes, there is considerable disagreement over the values for these constants (Dyrssen, 1988, Zhang and Millero, 1994, Luther et al., 1996, Al-Farawati and van den Berg, 1999). Finally, there have been numerous experimental studies of the hydrolysis of Co^{2+} at ambient temperature and stability constants for $CoOH^+$, $Co(OH)_2^o$, $Co(OH)_3^-$ and $Co(OH)_4^{2-}$ have been reported. These constants were rigorously evaluated by Plyasunova et al. (1998), who recommended a preferred set of values for them. Based on these values, the complexes are all weakly stable and, consequently, the simple ion, Co^{2+}, is the dominant species in aqueous fluids with low chloride and bisulfide contents, except at very high pH (>9).

There have been only three experimental studies of aqueous Co chloride complexation at elevated temperature, namely, those of Pan and Susak (1989), Liu et al. (2011), Migdisov et al. (2011). Only those of Liu et al. (2011) and Migdisov et al. (2011), however, considered temperatures above 90 ºC. These studies, which were all conducted at saturation vapour pressure, showed that Co forms stable complexes with up to four chloride ions, i.e., $CoCl^+$, $CoCl_2^o$, $CoCl_3^-$ and $CoCl_4^{2-}$. There is, however, considerable disagreement between Liu et al. (2011) and Migdisov et al. (2011) over the relative stability of these complexes except for $CoCl^+$; the data of Pan and Susak (1989) cannot be compared directly with those of Liu et al. (2011) and Migdisov et al. (2011) because the lowest temperature considered in the latter studies was 150 ºC. In the case of $CoCl_2^o$, part of the disagreement may arise from the fact that the study of Liu et al. (2011) reported separate formation constants for cobalt in four- and six-fold coordination, whereas and Migdisov et al. (2011) reported the bulk formation constants. The agreement is relatively good at 150 ºC and 300 ºC, for which

448 we surmise that $CoCl_2^o$ (the dominant species) is in octahedral and tetrahedral coordination,
449 respectively. In contrast, the formation constant reported by Migdisov et al. (2011) for $CoCl_2^o$ at
450 200 ºC is ~1 log unit higher than that reported by Liu et al. (2011). If, however, we sum the two
451 formation constants of Liu et al. (2011) for this temperature, the agreement is remarkably good.
452 Liu et al. (2011) did not report formation constants for $CoCl_3^-$. The disagreement between
453 Migdisov et al. (2011) and Liu et al. (2011) is greatest over the formation constant for $CoCl_4^{2-}$ and
454 reaches two orders in magnitude at 300 ºC, with the higher values being those of Migdisov et al.
455 (2011). The reason for this disagreement is unknown. As the formation constants reported by
456 Migdisov et al. (2011) were obtained by two independent methods (solubility and UV-
457 spectroscopy), both of which yielded similar values, we consider them to be more reliable than
458 those reported by Liu et al. (2011). There has been only one experimental study of Co bisulfide
459 speciation at hydrothermal conditions, namely that of Migdisov et al. (2011), who determined
460 values of the formation constant of $CoHS^+$ for temperature up to 300 ºC and saturated vapour
461 pressure. There also has been only one experimental study of Co hydrolysis at elevated temperature
462 (Giasson and Tewari, 1978). This study reported formation constants for $CoOH^+$ at temperatures
463 up to 200 ºC. Shock et al. (1997) fitted the data of Giasson and Tewari (1978) and used them to
464 determine the thermodynamic properties of this species. They also reported thermodynamic data
465 for $Co(OH)_2°$, $Co(OH)_3^-$ and $Co(OH)_4^{2-}$.

466 In order to determine the relative importance of Cl^-, HS^- and OH^- in the transport of cobalt, we
467 evaluated the speciation of Co in an aqueous fluid at 25, 150 and 300 ºC for a wide range of pH
468 (Fig. 6). The Cl^- activity was set at 1, the H_2S activity at 0.001 and the Co concentration at 0.01
469 M. As is evident from Figure 6a, $CoCl^+$ is the dominant species at 25 ºC for pH values between 1
470 and ~3.5, and that up to a pH of 3, $CoCl^+$ and Co^{2+} comprise >60 and ~20 % of the Co budget,
471 respectively. At a pH >3.5, $CoHS^+$ is the dominant species, and between a pH of 5 and 10 is the
472 only significant dissolved Co species. At 150 ºC, $CoCl_4^{2-}$ is the dominant Co species for pH values
473 up to ~7 (Fig. 6b). The next most abundant species up to a pH of ~6 is $CoCl_3^-$. Above this pH,
474 $CoHS^+$ makes up a significant proportion of the dissolved cobalt and is present in a proportion
475 similar to that of $CoCl_4^{2-}$ at a pH of 7. At higher pH, the proportion of $CoHS^+$ decreases sharply
476 and that of $CoCl_4^{2-}$ exceeds it, reaching a peak of ~70 % at a pH of 8. The latter is the dominant
477 species up to a pH ~8.5, above which it is replaced by $Co(OH)_2^o$ as the dominant species. This
478 species reaches a maximum of 88 % at a pH of 9.5. The Co speciation at 300 ºC is similar to that

at 150 ºC, i.e., $CoCl_4^{2-}$ is the dominant species for a wide range of pH (1-9.5). The major difference is that $CoCl_3^-$ and $CoHS^+$ do not make up a significant proportion of the Co budget (Fig. 6c). Above a pH 9.5, $CoCl_4^{2-}$ is replaced by $Co(OH)_3^-$ as the dominant species.

In principle, cobalt should also form stable chloride complexes in its 3+ state, but because Co^{3+} is a hard acid, these complexes are predicted to be considerably weaker than those formed with Co^{2+} (borderline acid, see above). Consequently, they are unlikely to contribute significantly to the solubility of cobalt in aqueous fluids. Cobalt in its 3+ state could form stable complexes with hydroxide. In order to determine whether significant cobalt can dissolve as 3+ hydroxide species, we estimated the solubility of cobalt metal in aqueous solutions with a chloride activity of 1 for pH values ranging from 1 to 10, assuming that fO_2 was buffered by the assemblage magnetite-hematite (MH). For the purpose of this exercise, cobalt was assumed to dissolve as $CoCl_4^{2-}$ (the dominant species at pH values up to ~7; see above), $CoOH^+$ and $CoOH^{2+}$ (the latter is the only cobalt 3+ complex for which there are thermodynamic data; Shock et al., 1997). As expected, the cobalt metal dissolved predominantly as $CoCl_4^{2-}$ to high pH and the relative importance of $CoOH^+$ increased with increasing pH. The contribution of $CoOH^{2+}$ to the overall cobalt solubility is many orders of magnitude less than that of $CoOH^+$ (e.g., 15 orders of magnitude less at 150 ºC) and this difference increases with increasing pH. This suggests that Co^{3+} will be insoluble in most natural aqueous fluids.

In summary, cobalt is predicted to be transported dominantly as chloride complexes, namely, $CoCl^+$ at 25 ºC and $CoCl_4^{2-}$ at temperatures above 150 ºC in aqueous fluids with a chloride activity of 1 and a total sulfur activity of 0.001. At lower Cl^- activity, the simple ion (Co^{2+}) may be important, particularly at low temperature and low to weakly acidic pH. The bisulfide species is likely to be important from slightly acidic to alkaline conditions but only at temperatures below ~150 ºC. Hydroxide species are unlikely to play a significant role in the aqueous transport of cobalt, except at unusually high pH.

Deposition

The main cobalt ore mineral at ambient temperature is heterogenite, which deposits either as a result of the formation of laterites during the weathering of olivine-rich ultramafic rocks (Freyssinet et al., 2005) or the supergene enrichment of magmatic and hydrothermal sulfide ores

(Fay and Barton, 2012). Erythrite forms from Co-arsenide and sulfarsenide ores but is not mined. The weathering fluids (meteoric waters) responsible for heterogenite formation are mildly to strongly acidic (supergene enrichment) and have low chlorinity. Consequently, Co is dissolved as the simple ion (Co^{2+}) and deposition proceeds according to the reaction:

$$Co^{2+} + 1.5\ H_2O + 0.25\ O_2 = CoOOH + 2\ H^+ \quad (3)$$

Heterogenite deposition, therefore, occurs either in response to an increase in fO_2 (needed to oxidize Co^{2+} to Co^{3+}) or an increase in pH, the dominant control (Vasyukova and Williams-Jones, 2021), during laterite formation.

Hydrothermal deposits form as a result of the precipitation of sulfides, sulfarsenides and arsenides. Globally, however, most of the production of cobalt is from sulfides. The arsenides and sulfarsenides are only important in a small number of deposits, notably, in the Bou Azzer district, Morocco, and the Cobalt district, Canada. Among the sulfides, the main ore minerals are carollite, cattierite, linnaeite and cobalt pentlandite. The parameters controlling the deposition of the sulfide minerals are temperature, fO_2, pH, the activity of reduced sulfur and the ligand activity.

Processes that can cause favorable changes in these parameters include fluid-rock interaction, boiling (or effervescence, i.e., exsolution of gas species, e.g., CO_2) and fluid mixing. Fluid-rock interaction will commonly lead to changes in pH and fO_2, and, in some cases, reduced sulfur activity. Boiling causes sharp drops in temperature in the residual liquid due to the much higher enthalpy of the vapor. As boiling/effervescence involves the separation of dissolved gases, this will also lead to an increase in fO_2 (loss of H_2) and pH (loss of CO_2 and SO_2) and a decrease in reduced sulfur activity (loss of H_2S). Fluid mixing may lead to changes in temperature, fO_2, pH, the activity of reduced sulfur and the ligand activity.

To understand the factors that control the deposition of Co minerals, we modelled the stability and solubility of cattierite, linnaeite, cobaltpentlandite, CoO and Co_3O_4 (the only cobalt solids, other than Co metal, for which there are thermodynamic data) in an aqueous fluid containing 1 M Cl^-, with a total S activity of 0.001 (ΣaS), at temperatures up to 500°C and pressures up to 1 kbar. The species $CoCl_4^{2-}$ was assumed to be the only form of dissolved Co at elevated temperature based on our evaluation of the aqueous speciation of Co (see above). Thermodynamic data for this species

were taken from Migdisov et al. (2011) and those for the other aqueous species were taken from the HCh database (Shvarov and Bastrakov, 1999). The thermodynamic data for the solids are listed in Table 5.

In Figure 7a, we show stability relationships among the above minerals as a function of temperature and pH. The diagram was constructed such that fO_2 was buffered to a value 5 log units below the MH buffer, which is roughly equivalent to the oxygen fugacity of the FMQ buffer. This fO_2 was chosen to reflect the fact that Co deposits commonly form in reduced environments, e.g., the black shales of the DRC. The pressure was assumed to be 1 kbar. The most important observations that can be drawn from Figure 7a are that Co-mineral solubility decreases with decreasing temperature and increasing pH, and that cobaltpentlandite is the first mineral to deposit at high temperature but only at pH values above ~7 (this assumes a maximum Co concentration in the fluid of 100 ppm). At lower pH, the solubility of Co is too high to saturate the fluid with cobaltpentlandite. With a further decrease in temperature and pH, the fluid saturates with linnaeite followed by cattierite. These observations help explain why, in the relatively low temperature hydrothermal deposits of the DRC, cattierite and linnaeite are common ore minerals, and cobaltpentlandite is rarely observed (Vasyukova and Williams-Jones, 2021). The three processes referred to above all could produce the required temperature decrease, but only boiling and fluid mixing would create sufficiently high thermal gradients necessary to produce a cobalt ore deposit by cooling alone.

In many hydrothermal systems, fO_2 and pH are major controls of ore deposition. Figures 7b and c has been constructed to help evaluate their potential role in cobalt ore formation. The most striking features of Figure 7b (150 ºC) are the remarkably sharp gradient in Co solubility with fO_2, the unusually high fO_2 of the solubility threshold (i.e., 2-4 log units above the magnetite-hematite buffer), and the very wide range of pH (2-8) for this threshold. There is also a sharp decrease in Co solubility with fO_2 at 300 ºC, but the range in pH over which this decrease in solubility occurs is much narrower, from ~6 to ~9 (Fig. 7c). These features lead to the conclusion that at low temperature (e.g., 150 ºC), Co is soluble only in highly oxidized hydrothermal fluids and will deposit in response to a very small decrease in fO_2 over a wide range of pH. At higher temperature (e.g., 300 ºC), Co is soluble in acidic fluids independent of whether they are oxidizing or reducing. In such fluids, Co-mineral deposition occurs in response to an increase in pH. At pH values

between 7 and 9, Co is only soluble in relatively oxidising fluids and Co-mineral deposition occurs in response to a decrease in fO_2 or an increase in pH.

Fluid-rock interaction and fluid mixing can both lead to the decrease in fO_2 required to induce Co-mineral deposition at low temperature (e.g., 150 ºC). In the former case, this could result from the interaction of the highly oxidized ore fluid with any rock containing a reducing agent, e.g., organic matter or ferro-magnesian minerals. Mixing of this ore fluid with a less oxidized fluid, e.g., a formational water that had equilibrated with black shale or ferro-magnesian mineral-bearing graywacke, would have the same effect.

The three processes mentioned above can all produce an increase in pH. In the case of fluid-rock interaction, carbonate rocks and unaltered to partially altered mafic and ultramafic rocks will buffer pH to the levels required for Co-mineral deposition at high temperature (at 300 ºC, this pH varies between 7 and 7.7 depending on fO_2). Indeed, calculations (using HCh software; Shvarov and Bastrakov, 1999) in which a 1M NaCl solution was equilibrated with limestone, dunite and an idealised basalt composition yielded pH values for the fluid of 7.8, 10.5 and 7.8-9.7 (depending on composition), respectively. By contrast, the same calculations for granite yielded a much lower pH of 5.9 which would be too low to induce Co-mineral deposition. Mixing of the ore fluid with a small amount of a high pH fluid could also lead to pH values sufficient to cause Co-mineral deposition at high temperature. For example, it would be only necessary to add 55 g of a fluid with a pH of 9 to 1 kg of an ore fluid with a pH of 5 to raise the pH to 7.7; if the pH of the former fluid were 8 the required amount of this fluid would rise to 1 kg. Although such high pH values are not typical, they are commonly reported from deep groundwaters equilibrating with mafic and ultramafic rocks (Nurmi et al., 1988, Gascoyne and Kamineni, 1994). Boiling is a particularly effective means of raising pH, as has been shown by numerous studies of geothermal waters. For example, Arnorsson et al. (1983) reported that reservoirs in high temperature geothermal fields in Iceland have near neutral pH, whereas boiling in some wells increases the pH to > 9 (see Table 1 in Arnorsson et al., 1983).

In addition to the unusually sharp gradient of cobalt solubility with fO_2, another striking feature of Figure 7b is the replacement of cattierite by linnaeite and, in turn, by cobaltpentlandite with increasing pH. Significantly, this corresponds to the paragenesis of Co minerals in some sediment-

595 hosted Cu-Co deposits, in which cattierite is replaced by linnaeite, and cobaltpentlandite is more
596 distal to fluid source than linnaeite (Vasyukova and Williams-Jones, 2021).

597 In principle, sulfur activity could also exercise a major control on Co mineralization. As shown in
598 Figure 7d, Co-sulfide mineral solubility decreases sharply with increasing ΣaS and, thus, Co ore
599 formation might occur, if the ore fluid interacted with a reduced sulfur-bearing rock, such as a
600 pyritiferous shale, or mixed with a euxinic (H_2S-rich) fluid. These processes, however, would lead
601 to either monomineralic Co-sulfide deposition or a paragenesis opposite to that commonly
602 observed, e.g., linnaeite followed by cattierite (see Fig. 7d). Although processes like sulfidation
603 (replacement of Fe-bearing silicate minerals by pyrite) and boiling (loss of H_2S or SO_2 to the vapor)
604 will lead to a decrease in ΣaS, promoting Co-sulfide mineral dissolution, a ΣaS decrease could also
605 accompany Co-mineral deposition, if coupled with an increase in pH. Moreover, it would also
606 produce the Co-mineral paragenesis observed in the DRC (red dashed arrow in Fig. 7d).

607 An unusual feature of the system Co-S-O is that the stable cobalt oxide mineral for a wide range
608 of fO_2 is CoO and that Co_3O_4 is stable only at fO_2 conditions well above the MH buffer (e.g., ~10
609 log units at 300 ºC). Indeed, CoO is stable to a fO_2 orders of magnitude above the upper limit of
610 stability of the corresponding iron oxide, wüstite (e.g., 14 log units at 300 ºC). The likely reason
611 for this unusual behavior of cobalt is its much higher first ionization potential relative to that of
612 iron, which makes it more difficult to oxidize (see section on properties of cobalt). Somewhat
613 surprisingly, however, the CoO phase has not been reported to occur naturally, whereas Co_3O_4
614 (guite) has been observed in trace quantities in the DRC (Lei et al., December 2017).

615 As noted earlier, there are no thermodynamic data for the Co-arsenides and -sulfarsenides, and
616 consequently, it is not possible to quantitatively evaluate the conditions that will promote their
617 deposition. It is, however, possible to determine their stability relationships qualitatively for some
618 parameters, e.g., fO_2 and pH, using the Gibbs-Duhem equation and chemographic analysis (Zen,
619 1966). In Figures 8 and 9, we present qualitative logfO_2-pH diagrams showing the stability
620 relationships among safflorite, skutterudite and cobaltite, and the Co-sulfide and -oxide minerals
621 discussed earlier. The diagrams in these figures were constructed assuming that the dissolved
622 sulfur species are H_2S, HS^-, HSO_4^- and SO_4^{2-} and As is present as the species $H_3AsO_3^0$. In both
623 figures, diagrams (a) to (d) are ordered to show the effects of a progressive increase in the As/S

ratio. In Figure 8, however, this increase in the As/S ratio corresponds to an increase in the activity of $H_3AsO_3^0$ and a decrease in the activity of dissolved sulfur, whereas in Figure 9, the activity of dissolved sulfur is constant. The reason for preparing the second figure is that there is evidence for some cobalt arsenide deposits that the total sulfur activity was relatively high and constant despite the absence of cobalt sulfide minerals (Vasyukova and Williams-Jones, 2021).

From Figure 8, it is evident that the arsenide minerals are stable at fO_2 conditions below those at which the sulfide minerals are stable, and that at low As/S they are separated from the latter by the sulfarsenide, cobaltite (Fig. 8a). With an increase in As/S, the skutterudite-safflorite stability boundary moves to higher fO_2 and the cobaltite stability field shrinks, ultimately disappearing (Fig. 8b and c). This change in stability relationships is accompanied by decreases in the sizes of the sulfide stability fields and the sequential disappearance of the stability fields for cattierite, linnaeite and cobaltpentlandite (Fig. 8c and d). An important conclusion that can be drawn from Figure 8 is that Co-sulfides are unlikely to co-precipitate with Co-arsenides, i.e., if the fO_2 conditions of deposition are consistent with the stability of the sulfides, arsenide precipitation is inhibited because of the restriction of the Co-arsenide minerals to lower fO_2. Conversely, the As/S ratio required for arsenide minerals to be stable at the higher fO_2 precludes saturation of the fluid with Co-sulfide minerals. This explains why Co-sulfide minerals are rarely observed to coexist with Co-arsenide minerals. Another conclusion is that, at these conditions, fO_2 exercises a major control on Co-mineral stability.

Figure 9 differs from Figure 8 mainly in the behavior of cobaltite. Whereas the stability field of cobaltite disappears with increasing As/S ratio in Figure 8, bringing safflorite into direct contact with cobaltpentlandite, in Figure 9, the upper boundary of the field of cobaltite expands at the expense of the Co sulfides and, at very high As/S ratio, cobaltite replaces them (cobaltpentlandite followed by linnaeite and cattierite). Thus, in cases where the S content is high and the high As/S ratio is controlled by As, cobalt sulfides will not be stable in the presence of cobalt arsenides. An important conclusion that can be drawn from Figure 9 is that, at high As activity, pH exercises a major control on the nature of the stable Co-mineral, i.e., with limited change in fO_2, Co sulfides are stable at low pH, and with increasing pH are replaced by cobaltite and, in turn, safflorite.

To summarize, at ambient temperature cobalt is transported as the simple ion, Co^{2+}, and precipitates as the oxy-hydroxide, Co^{3+} mineral, heterogenite, either as a result of the oxidation of primary hydrothermal ores or during the weathering of olivine-rich ultramafic rocks to laterite. In both cases, increasing pH is a major cause of ore mineral deposition (Vasyukova and Williams-Jones, 2021). At hydrothermal conditions, cobalt is transported dominantly as the species $CoCl_4^{2-}$ and deposited as sulfide minerals, except at high As activity (and/or extremely low fO_2). The main control on Co-sulfide deposition at low temperature (e.g., 150 °C) is a decrease in fO_2, whereas at higher temperature, ore deposition is controlled primarily by increasing pH. Changes in the activity of reduced sulfur play a subordinate role, and decreasing reduced sulfur activity, caused by processes like sulfidation (important in gold ore genesis) actually inhibits cobalt ore formation, unless coupled with an increase in pH. At high As activity, Co-sulfide minerals are replaced by Co-sulfarsenides and -arsenides. Although an absence of thermodynamic data precludes a discussion of their solubility, chemographic analysis shows that the Co-arsenides are stable at lower fO_2 than the Co-sulfides, that with increasing As/S they replace the Co-sulfides and that at constant S activity, relatively constant fO_2, and high As activity, increasing pH is marked by the replacement of Co sulfides by Co-sulfarsenites and, in turn, Co-arsenides.

Conclusions

Cobalt is a compatible metal that reaches its highest concentration in olivine and, thus, in rocks of ultramafic and, to a lesser extent, mafic composition. Economic deposits of Co, therefore, develop as a result of processes involving ultramafic/mafic magmas and rocks. These processes comprise silicate/sulfide liquid immiscibility, hydrothermal mobilization and weathering. Magmatic Co ores are the products of the separation from ultramafic and mafic magmas of small proportions of sulfide liquid into which the Co partitions strongly and is accompanied by much larger proportions of Ni. Ore formation occurs as a result of the crystallization monosulfide solid solution, into which Co partitions preferentially, and the exsolution from MSS of pentlandite, the main Co ore mineral.

Hydrothermally, Co is transported mainly as a chloride complexes ($CoCl_4^{2-}$), which is stable at low pH and high fO_2, and deposits as sulfide, sulfarsenide and arsenide minerals. Based on an evaluation of phase and solubility relationships for cobalt sulfides (there are no thermodynamic data available for cobalt arsenides and sulfarsenides), the main cause of ore mineral deposition is a reduction in fO_2, particularly at the comparatively low temperature of formation of sediment-

hosted deposits. At higher temperature, increasing pH is more important. Chemographic analysis conducted in tandem with knowledge of the aqueous speciation of As, indicates that Co-sulfarsenides and -arsenides are stable at lower fO_2 than Co-sulfides, that Co-sulfarsenides (cobaltite) are stable at fO_2 conditions intermediate to those of the sulfides and arsenides and, therefore, that the latter two groups of minerals cannot coexist (except if an extremely high activity of arsenic is accompanied by extremely low activity of sulfur). This analysis also shows that at a high As/S ratio, one favoring the deposition of Co-arsenides over Co-sulfides, Co-arsenides and sulfarsenides are stable even at relatively high fO_2.

At ambient temperature, Co is transported dominantly as chloride species ($CoCl^+$), except in low chloride aqueous fluids such as the meteoric waters that are responsible for the formation of laterite Co deposits or the supergene enrichment of primary magmatic or hydrothermal Co deposits. In these examples, the water is mildly acidic and the Co is transported primarily as the simple ion, Co^{2+}. Mineral deposition, e.g., as the mineral heterogenite, is favoured by increasing fO_2 due to the oxidation of Co^{2+} to Co^{3+}, and increasing pH.

To summarize, Co deposits ultimately owe their origin to ultramafic and to a lesser extent mafic magmas/rocks and acquire economic concentrations of this metal either through its affinity for sulfur (sulfide-silicate liquid immiscibility) or as a result of its mobilization by aqueous fluids of high or low temperature at favourable conditions of pH, fO_2 and chloride activity. In a companion study (Vasyukova and Williams-Jones, 2021), we use the findings presented here, in conjunction with published geological information, to develop/refine genetic models for the principal cobalt deposit-types that we hope will aid the discovery of new resources of this critical metal.

Acknowledgements

The research presented in this paper was funded by a Discovery grant from the National Scientific and Engineering Research Council of Canada (NSERC).

Figure captions

Figure 1. a) The main uses of cobalt; b) Current and predicted future demand for cobalt as a function of use. Modified from Alves Dias et al. (2018).

Figure 2. Cobalt resources as a function of deposit type. Modified from Slack (2017).

Figure 3. Cobalt mineral-melt partition coefficients for olivine (black), orthopyroxene (red) and clinopyroxene (blue) as a function of the MgO content of the magma. The horizontal dashed line indicates equal partitioning of cobalt into mineral and melt. The intersections of this line with the partition coefficient curves for the minerals indicate the MgO content of the magma, below which Co prefers the mineral (vertical dashed lines). The partition coefficients were calculated from the data of Bedard (2005, 2007 and 2014).

Figure 4. The modeled Co content of the magma (green), the percent magma crystallized (red) and the Co content of the crystal cumulate (black) with decreasing temperature during the fractional crystallization of: a) a komatiitic magma and b) a basaltic magma. This modeling was carried out using the computer program, Pele (Boudreau, 1999). See main text for further explanation.

Figure 5. A comparison of measured Co sulfide-silicate partition coefficients to those predicted using Equation (5) in Li and Audétat (2015).

Figure 6. The aqueous speciation of Co as a function of pH for a fluid with a Cl^- activity of 1, a H_2S activity of 0.001 and a Co concentration of 0.01 M at: a) 25 °C, b 150 °C and c) 300 °C. The thermodynamic data for Co^{2+} were taken from Shock et al. (1997), the data for the hydroxide species from Pyasunova et al. (1998) and the chloride and bisulfide species from Migdisov et al. (2011).

Figure 7. Stability relationships for the Co minerals, cattierite (CoS_2), linnaeite (Co_3S_4), cobaltpentlandite (Co_9S_8) and guite (Co_3O_4) and the solid, CoO, as a function of a) temperature and pH, b) log fO_2 and pH at 150 °C, c) log fO_2 and pH at 300 °C, and d) log ΣaS and pH at 150 °C. Also shown are the predominance boundaries for aqueous sulfur species and solubility contours for the cobalt minerals assuming that Co was dissolved as the species $CoCl_4^{2-}$. The thermodynamic data for the minerals shown in these diagrams are reported in Table 5 and the thermodynamic data for $CoCl_4^{2-}$ were taken from Migdisov et al. (2012). All other thermodynamic data were taken from the database in the HCh software package (Shvarov, 1999). The horizontal black dashed line in (b) and (c) is the MH buffer.

Figure 8. Diagrams showing the stability relationships of the sulfide and oxide minerals/phase considered in Figure 7, the sulfaresenide, cobaltite (CoAs), and the arsenides, safflorite ($CoAs_2$) and skutterudite ($CoAs_3$) as a function of fO_2 and pH. They were constructed using chemographic analysis, in which the slopes of the stability boundaries were determined by the Gibbs Duhem equation and their relative locations were dictated by the direction of redox and pH changes across these boundaries. This construction assumed that the dissolved sulfur species are H_2S, HS^-, HSO_4^- and SO_4^{2-} and As is present as the species $H_3AsO_3^0$. The diagrams are ordered from a) to d) to reflect a progressive increase in the activity of As and a corresponding decrease in the activity of S.

Figure 9. Stability relationships as a function of fO_2 and pH for the phases considered in Figure 8. They are ordered from a) to d) to reflect a progressive increase in the activity of As at constant activity of S.

Acknowledgements

The research presented in this paper was funded by a Discovery grant from the National Scientific and Engineering Research Council of Canada (NSERC).

References

Al-Farawati, R., and van den Berg, C. M. G., 1999, Metal-sulfide complexation in seawater: Marine Chemistry, v. 63, p. 331-352.

Alves Dias, P., Arvanitidis, N., Blagoeva, D., and Pavel, C., 2018, Cobalt: Demand-supply balances in the transition to electric mobility, Publications Office of the European Union.

Arndt, N. T., and Jenner, G. A., 1986, Crustally contaminated komatiites and basalts from Kambalda, Western Australia: Chemical Geology, v. 56, p. 229-255.

Arnorsson, S., Gunnlaugsson, E., and Svavarsson, H., 1983, The Chemistry of Geothermal Waters in Iceland .2. Mineral Equilibria and Independent Variables Controlling Water Compositions: Geochimica Et Cosmochimica Acta, v. 47, p. 547-566.

Barin, I., Knacke, O., and Kubaschewski, O., 1977, Thermodynamic properties of inorganic substances, Springer-Verlag Berlin Heidelberg.

Barnes, S.-J., and Lightfoot, P. C., 2005, Formation of magmatic nickel sulfide deposits and processes affecting their copper and platinum group element contents, One Hundredth Anniversary Volume, Society of Economic Geologists, p. 0.

Bedard, J. H., 2005, Partitioning coefficients between olivine and silicate melts: Lithos, v. 83, p. 394-419.

Bedard, J. H., 2007, Trace element partitioning coefficients between silicate melts and orthopyroxene: parameterizations of D variations: Chemical Geology, v. 244, p. 263-303.

Bedard, J. H., 2014, Parameterizations of calcic clinopyroxene - melt trace element partition coefficients: Geochemistry Geophysics Geosystems, v. 15, p. 303-336.

Berger, V. I., Singer, D. A., Bliss, J. D., and Moring, B. C., 2011, Ni-Co Laterite Deposits of the World - Database and Grade and Tonnage Models, U.S. Geological Survey, Open-File Report 2011-1058, http://pubs.usgs.gov/of/2011/1058/.

Berzelius, J. J., 1818, Lärobok i Kemien (Textbook in Chemistry): Stockholm, 496 p.

Bouabdellah, M., Maacha, L., Levresse, G., and Saddiqi, O., 2016, The Bou Azzer Co–Ni–Fe–As(±Au ± Ag) District of Central Anti-Atlas (Morocco): A Long-Lived Late Hercynian to Triassic Magmatic-Hydrothermal to Low-Sulphidation Epithermal System, *in* Bouabdellah, M., and Slack, J. F., eds., Mineral Deposits of North Africa: Cham, Springer International Publishing, p. 229-247.

Boudreau, A. E., 1999, PELE - a version of the MELTS software program for the PC platform: Computers and Geosciences, v. 25, p. 201-203.

Brooker, R. A., and Kjarsgaard, B. A., 2011, Silicate-carbonate liquid immiscibility and phase relations in the system SiO_2-Na_2O-Al_2O_3-CaO-CO_2 at 0.1-2.5 GPa with applications to carbonatite genesis: Journal of Petrology, v. 52, p. 1281-1305.

Cailteux, J. L. H., Kampunzu, A. B., Lerouge, C., Kaputo, A. K., and Milesi, J. P., 2005, Genesis of sediment-hosted stratiform copper–cobalt deposits, central African Copperbelt: Journal of African Earth Sciences, v. 42, p. 134-158.

Carroll, M. R., and Rutherford, M. J., 1988, Sulfur speciation in hydrous experimental glasses of varying oxidation state; results from measured wavelength shifts of sulfur X-rays: American Mineralogist, v. 73, p. 845-849.

Cottrell, E., and Kelley, K. A., 2011, The oxidation state of Fe in MORB glasses and the oxygen fugacity of the upper mantle: Earth and Planetary Science Letters, v. 305, p. 270-282.

Dalton, J., 1808, A new system of chemical philisophy: London, 566 p.

Dolansky, L. M., 2007, Controls on the genesis of hydrothermal cobalt mineralization: insights from the mineralogy and geochemistry of the Bou Azzer deposits, Morocco, McGill University Libraries, 192 p.

802 Duan, Z. H., Moller, N., and Weare, J. H., 1992, Molecular-dynamics simulation of PVT
803 properties of geological fluids and a general equation of state of nonpolar and weakly polar
804 gases up to 2000-K and 20,000 bar: Geochimica et Cosmochimica Acta, v. 56, p. 3839-
805 3845.

806 Dyrssen, D., 1988, Sulfide Complexation in Surface Seawater: Marine Chemistry, v. 24, p. 143-
807 153.

808 Eby, G. N., 1979, Mount-Johnson, Quebec - example of silicate-liquid immiscibility: Geology, v.
809 7, p. 491-494.

810 Elkins-Tanton, L. T., Grasby, S. E., Black, B. A., Veselovskiy, R. V., Ardakani, O. H., and
811 Goodarzi, F., 2020, Field evidence for coal combustion links the 252 Ma Siberian Traps
812 with global carbon disruption: Geology, v. 48, p. 986-991.

813 En-Naciri, A., Barbanson, L., and Touray, J.-C., 1997, Brine inclusions from the Co-As(Au) Bou
814 Azzer District, Anti-Atlas Mountains, Morocco: Economic Geology, v. 92, p. 360-367.

815 Eugster, H. P., 1986, Minerals in Hot Water: American Mineralogist, v. 71, p. 655-673.

816 Fay, I., and Barton, M. D., 2012, Alteration and ore distribution in the Proterozoic Mines Series,
817 Tenke-Fungurume Cu–Co district, Democratic Republic of Congo: Mineralium Deposita,
818 v. 47, p. 501-519.

819 Freyssinet, P., Butt, C. R. M., Morris, R. C., and Piantone, P., 2005, Ore-forming processes related
820 to lateritic weathering, *in* Hedenquist, J. W., Thomson, J. F. H., Goldfarb, R. J., and
821 Richards, J. P., eds., Economic Geology 100th Anniversary Volume, Economic Geology
822 Publishing Company, New Haven, Connecticut, p. 681-722.

823 Gaetani, G. A., and Grove, T. L., 1997, Partitioning of moderately siderophile elements among
824 olivine, silicate melt, and sulfide melt: Constraints on core formation in the Earth and Mars:
825 Geochimica Et Cosmochimica Acta, v. 61, p. 1829-1846.

826 Gascoyne, M., and Kamineni, D. C., 1994, The Hydrogeochemistry Of Fractured Plutonic Rocks
827 In The Canadian Shield: Applied Hydrogeology, v. 2, p. 43-49.

828 Giasson, G., and Tewari, P. H., 1978, Hydrolysis of Co(II) at eevated temperatures: Canadian
829 Journal of Chemistry-Revue Canadienne De Chimie, v. 56, p. 435-440.

830 Halter, W. E., Pettke, T., and Heinrich, C. A., 2002, The origin of Cu/Au ratios in porphyry-type
831 ore deposits: Science, v. 296, p. 1844-1846.

832 Holloway, J. R., Pan, V., and Gudmundsson, G., 1992, High-pressure fluid-absent melting
833 experiments in the presence of graphite; oxygen fugacity, ferric/ferrous ratio and dissolved
834 CO 2: European Journal of Mineralogy, v. 4, p. 105-114.

835 Huppert, H. E., Sparks, R. S. J., Turner, J. S., and Arndt, N. T., 1984, Emplacement and cooling
836 of komatiite lavas: Nature, v. 309, p. 19-22.

Johnson, M. C., Anderson, A. T., and Rutherford, M. J., 1994, Pre-Eruptive Volatile Contents of Magmas: Volatiles in Magmas, v. 30, p. 281-330.

Jugo, P. J., Luth, R. W., and Richards, J. P., 2005, An Experimental Study of the Sulfur Content in Basaltic Melts Saturated with Immiscible Sulfide or Sulfate Liquids at 1300°C and 1·0 GPa: Journal of Petrology, v. 46, p. 783-798.

Keith, J. D., Whitney, J. A., Hattori, K., Ballantyne, G. H., Christiansen, E. H., Barr, D. L., Cannan, T. M., and Hook, C. J., 1997, The role of magmatic sulfides and mafic alkaline magmas in the Bingham and Tintic mining districts, Utah: Journal of Petrology, v. 38, p. 1679-1690.

Kiseeva, E. S., and Wood, B. J., 2013, A simple model for chalcophile element partitioning between sulphide and silicate liquids with geochemical applications: Earth and Planetary Science Letters, v. 383, p. 68-81.

Kjarsgaard, B. A., and Hamilton, D. L., 1988, Liquid immiscibility and the origin of alkali-poor carbonatites: Mineralogical Magazine, v. 52, p. 43-55.

Krivolutskaya, N. A., Kuzmin, D. V., Gongalsky, B. I., Roshchina, I. A., Kononkova, N. N., Svirskaya, N. M., and Romashova, T. V., 2018, Stages of Trap Magmatism in the Norilsk Area: New Data on the Structure and Geochemistry of the Volcanic Rocks: Geochemistry International, v. 56, p. 419-437.

Lebas, M. J., 1981, Carbonatite magmas: Mineralogical Magazine, v. 44, p. 133-140.

Lei, Z., Chen, X., Wang, J., Zhang, J., Huang, Y., Lu, Z., and Du, F., December 2017, Guite, IMA 2017-080. CNMNC Newsletter No. 40, : Mineralogical Magazine, v. 81, p. 1581.

Lester, G. W., Kyser, T. K., Clark, A. H., and Layton-Matthews, D., 2013, Trace element partitioning between immiscible silicate melts with H_2O, P, S, F, and Cl: Chemical Geology, v. 357, p. 178-185.

Li, Y., and Audétat, A., 2015, Effects of temperature, silicate melt composition, and oxygen fugacity on the partitioning of V, Mn, Co, Ni, Cu, Zn, As, Mo, Ag, Sn, Sb, W, Au, Pb, and Bi between sulfide phases and silicate melt: Geochimica et Cosmochimica Acta, v. 162, p. 25-45.

Lightfoot, P. C., Hawkesworth, C. J., Hergt, J., Naldrett, A. J., Gorbachev, N. S., Fedorenko, V. A., and Doherty, W., 1993, Remobilisation of the continental lithosphere by a mantle plume: major-, trace-element, and Sr-, Nd-, and Pb-isotope evidence from picritic and tholeiitic lavas of the Noril'sk District, Siberian Trap, Russia: Contributions to Mineralogy and Petrology, v. 114, p. 171-188.

Liu, W. H., Borg, S. J., Testemale, D., Etschmann, B., Hazemann, J. L., and Brugger, J., 2011, Speciation and thermodynamic properties for cobalt chloride complexes in hydrothermal fluids at 35-440 degrees C and 600 bar: An in-situ XAS study: Geochimica Et Cosmochimica Acta, v. 75, p. 1227-1248.

873 Luther, G. W., Rickard, D. T., Theberge, S., and Olroyd, A., 1996, Determination of metal
874 (Bi)sulfide stability constants of Mn^{2+}, Fe^{2+}+, Co^{2+}, Ni^{2+}, Cu^{2+}, and Zn^{2+} by voltammetric
875 methods: Environmental Science & Technology, v. 30, p. 671-679.

876 Martin, L. H. J., Schmidt, M. W., Mattsson, H. B., and Guenther, D., 2013, Element partitioning
877 between immiscible carbonatite and silicate melts for dry and H_2O-bearing systems at 1-3
878 GPa: Journal of Petrology, v. 54, p. 2301-2338.

879 Mavrogenes, J. A., and O'Neill, H. S. C., 1999, The relative effects of pressure, temperature and
880 oxygen fugacity on the solubility of sulfide in mafic magmas: Geochimica et
881 Cosmochimica Acta, v. 63, p. 1173-1180.

882 Migdisov, A. A., Zezin, D., and Williams-Jones, A. E., 2011, An experimental study of Cobalt
883 (II) complexation in Cl- and H2S-bearing hydrothermal solutions: Geochimica et
884 Cosmochimica Acta, v. 75, p. 4065-4079.

885 Mills, K. C., 1974, Thermodynamic data for inorganic sulphides, selenides and tellurides: United
886 Kingdom, Butterworths.

887 Mitchell, A. L., Gaetani, G. A., O'Leary, J. A., and Hauri, E. H., 2017, H_2O solubility in basalt at
888 upper mantle conditions: Contributions to Mineralogy and Petrology, v. 172.

889 Nadeau, O., Williams-Jones, A. E., and Stix, J., 2010, Sulphide magma as a source of metals in
890 arc-related magmatic hydrothermal ore fluids: Nature Geoscience, v. 3, p. 501-505.

891 Naldrett, A. J., 2004a, Komatiite-Related Deposits, *in* Naldrett, A. J., ed., Magmatic Sulfide
892 Deposits: Geology, Geochemistry and Exploration: Berlin, Heidelberg, Springer Berlin
893 Heidelberg, p. 67-136.

894 Naldrett, A. J., 2004b, Ore deposits associated with flood basalt volcanism, Magmatic Sulfide
895 Deposits: Geology, Geochemistry and Exploration: Berlin, Heidelberg, Springer Berlin
896 Heidelberg, p. 137-278.

897 Naldrett, A. J., 2004c, Theoretical considerations, Magmatic Sulfide Deposits: Geology,
898 Geochemistry and Exploration: Berlin, Heidelberg, Springer Berlin Heidelberg, p. 21-66.

899 Nurmi, P. A., Kukkonen, I. T., and Lahermo, P. W., 1988, Geochemistry and origin of saline
900 groundwaters in the Fennoscandian Shield: Applied Geochemistry, v. 3, p. 185-203.

901 Palme, H., and O'Neill, H. S., 2014, Cosmochemical estimates of mantle composition, *in* Rudnick,
902 R. L., ed., Treatise on Geochemistry, 3: Oxford, Elsevier.

903 Pan, P., and Susak, N. J., 1989, Co(II)-chloride and Co(II)-bromide complexes in aqueous-
904 solutions up to 5m NaX and 90-Degrees-C - Spectrophotometric study and geological
905 Implications: Geochimica Et Cosmochimica Acta, v. 53, p. 327-341.

906 Pankratz, L. B., Mah, A. D., and Watson, S. W., 1987, Thermodynamic properties of sulfides,
907 Bulletine/United States Depatments of the Interior, Bureau of Mines; 689, 424 p.

Patten, C., Barnes, S.-J., Mathez, E. A., and Jenner, F. E., 2013, Partition coefficients of chalcophile elements between sulfide and silicate melts and the early crystallization history of sulfide liquid: LA-ICP-MS analysis of MORB sulfide droplets: Chemical Geology, v. 358, p. 170-188.

Peach, C. L., Mathez, E. A., and Keays, R. R., 1990, Sulfide melt-silicate melt distribution coefficients for noble metals and other chalcophile elements as deduced from MORB: Implications for partial melting: Geochimica Et Cosmochimica Acta, v. 54, p. 3379-3389.

Pearson, R. G., 1963, Hard and soft acids and bases: Journal of the American Chemical Society, v. 85, p. 3533-3539.

Philpotts, A. R., 1972, Density, surface tension and viscosity of the immiscible phase in a basic, alkaline magma: Lithos, v. 5, p. 1-18.

Plyasunova, N. V., Zhang, Y., and Muhammed, M., 1998, Critical evaluation of thermodynamics of complex formation of metal ions in aqueous solutions. IV. Hydrolysis and hydroxo-complexes of Ni2+ at 298.15 K: Hydrometallurgy, v. 48, p. 43-63.

Robie, A., and Hemingway, B. S., 1995, Thermodynamic properties of minerals and related substances at 298.15 K and 1 bar (10^5 pascals) pressure and at higher temperatures: Washington, U.S. geological survey bulletin 2131.

Roedder, E., and Weiblen, P. W., 1970, Silicate liquid immiscibility in lunar magmas, evidenced by melt inclusions in lunar rocks: Science, v. 167, p. 641-644.

Rudnick, R. L., and Gao, S., 2014, Composition of the continental crust., *in* Turekian, K. K., and Holland, H. D., eds., Treatise on Geochemistry, 4: Oxford, Elsevier, p. 1-51.

Shock, E. L., Sassani, D. C., Willis, M., and Sverjensky, D. A., 1997, Inorganic species in geologic fluids: Correlations among standard molal thermodynamic properties of aqueous ions and hydroxide complexes: Geochimica et Cosmochimica Acta, v. 61, p. 907-950.

Shvarov, Y. V., 1999, Algorithmization of the numeric equilibrium modeling of dynamic geochemical processes: Geokhimiya, p. 646-652.

Shvarov, Y. V., and Bastrakov, E. N., 1999, HCh: a software package for geochemical equilibrium modelling. User's Guide.: Record 1999/25, Australian Geological Survey Organisation, 61 p.

Sillitoe, R. H., 2003, Iron oxide-copper-gold deposits: an Andean view: Mineralium Deposita, v. 38, p. 787-812.

Simon, A. C., Pettke, T., Candela, P. A., Piccoli, P. M., and Heinrich, C. A., 2004, Magnetite solubility and iron transport in magmatic-hydrothermal environments: Geochimica Et Cosmochimica Acta, v. 68, p. 4905-4914.

Sisson, T. W., and Layne, G. D., 1993, H_2O in basalt and basaltic andesite glass inclusions from 4 subduction-related volcanos: Earth and Planetary Science Letters, v. 117, p. 619-635.

Slack, J. F., Kimball, B. E., and Shedd, K. B., 2017, Critical mineral resources of the United States—Economic and environmental geology and prospects for future supply, *in* Schulz, K. J., DeYoung, J. J. H., Seal Ii, R. R., and Bradley, D. C., eds., Professional Paper: Reston, VA, p. 862.

Sluzhenikin, S. F., Krivolutskaya, N. A., Rad'ko, V. A., Malitch, K. N., Distler, V. V., and Fedorenko, V. A., 2014, Ultramafic-mafic intrusions, volcanic rocks and PGE-Cu-Ni sulfide deposits of the Noril'sk Province, Polar Siberia. Field trip guidebook: 12th International Platinum Symposium, Yekaterinburg, 2014, p. 80.

Soloviev, S. G., Kryazhev, S. G., and Dvurechenskaya, S. S., 2013, Geology, mineralization, stable isotope geochemistry, and fluid inclusion characteristics of the Novogodnee-Monto oxidized Au-(Cu) skarn and porphyry deposit, Polar Ural, Russia: Mineralium Deposita, v. 48, p. 603-627.

Sproule, R. A., Lesher, C. M., Ayer, J. A., Thurston, P. C., and Herzberg, C. T., 2002, Spatial and temporal variations in the geochemistry of komatiites and komatiitic basalts in the Abitibi greenstone belt: Precambrian Research, v. 115, p. 153-186.

Stuve, J. M., Beyer, R. P., and Brown, R. R., 1985, Thermodynamic properties of $CoS_{0.89}$, $CoS_{1.33}$, and CoS_2.

Vasyukova, O. V., and Williams-Jones, A. E., 2021, Constrains on the genesis of cobalt deposits: Part II, application to natural systems: Economic Geology

Veksler, I. V., Dorfman, A. M., Dulski, P., Kamenetsky, V. S., Danyushevsky, L. V., Jeffries, T., and Dingwell, D. B., 2012, Partitioning of elements between silicate melt and immiscible fluoride, chloride, carbonate, phosphate and sulfate melts, with implications to the origin of natrocarbonatite: Geochimica et Cosmochimica Acta, v. 79, p. 20-40.

Veksler, I. V., Petibon, C., Jenner, G. A., Dorfman, A. M., and Dingwell, D. B., 1998, Trace element partitioning in immiscible silicate-carbonate liquid systems: An initial experimental study using a centrifuge autoclave: Journal of Petrology, v. 39, p. 2095-2104.

Wang, S. Q., and Williams, P. J., 2001, Geochemistry and origin of Proterozoic skarns at the Mount Elliott Cu-Au(-Co-Ni) deposit, Cloncuny district, NW Queensland, Australia: Mineralium Deposita, v. 36, p. 109-124.

Webster, J. D., Kinzler, R. J., and Mathez, E. A., 1999, Chloride and water solubility in basalt and andesite melts and implications for magmatic degassing: Geochimica Et Cosmochimica Acta, v. 63, p. 729-738.

Weidendorfer, D., Schmidt, M. W., and Mattsson, H. B., 2016, Fractional crystallization of Si-undersaturated alkaline magmas leading to unmixing of carbonatites on Brava Island (Cape

Verde) and a general model of carbonatite genesis in alkaline magma suites: Contributions to Mineralogy and Petrology, v. 171.

White, W. M., and Klein, E. M., 2014, Composition of the oceanic crust, *in* Rudnick, R. L., ed., Treatise on Geochemistry, 4: Oxford, Elsevier, p. 457-496.

Williams-Jones, A. E., and Migdisov, A. A., 2014, Experimental constraints on the transport and deposition of metals in ore-forming hydrothermal systems: Building Exploration Capability for the 21st Century, p. 77-95.

Zen, E. a., 1966, Construction of pressure-temperature diagrams for multicomponent systems after the method of Schreinemakers - a geometric approach, Bulletin.

Zhang, J. Z., and Millero, F. J., 1994, Investigation of metal sulfide complexes in sea-water using cathodic stripping square-wave voltammetry: Analytica Chimica Acta, v. 284, p. 497-504.

Table 1. Commonly reported hypogene and supergene cobalt minerals and their formulae

1	Hypogene	Alloclasite	$(Co_{1-x}Fe_x)AsS$
3		Carrollite	$Cu(Co,Ni)_2S_4$
4		Cattierite	CoS_2
5		Clinosafflorite	$CoAs_2$
6		Cobaltite	CoAsS
7		Cobaltpentlandite	$(Co,Ni,Fe)_9S_8$
9		Glaucodot	$(Co_{0.50}Fe_{0.50})AsS$
10		Linnaeite	$Co^{2+}Co^{3+}{}_2S_4$
12		Modderite	(Co,Fe)As
14		Safflorite	$(Co,Ni,Fe)As_2$
15		Siegenite	$CoNi_2S_4$
16		Skutterudite	$CoAs_3$
17	Supergene	Asbolane	$(Ni,Co)_{2-x}Mn^{4+}(O,OH)_4 \cdot nH_2O)$
18		Erythrite	$Co_3(AsO_4) \cdot 2.8H_2O$
19		Heterogenite	CoO(OH)

Table 2. The compositions of komatiitic and basaltic magmas used in modeling the evolution of the Co content of the magmas during fractional crystallization.

	Komatiite[1]	Siberian flood basalts[2]
SiO_2	47.6	51.3
TiO_2	0.0	1.0
Al_2O_3	6.7	15.5
FeO	11.1	10.1
MnO	0.2	0.2
MgO	27.0	7.5
CaO	6.9	11.0
Na_2O	0.2	2.1
K_2O	0.02	0.6
P_2O_5	0.03	0.1
H_2O	0.2	0.2
Totals	100	99.7
Co, ppm	104	44

[1] - Sproule et al. (2002).
[2] - Krivolutskaya et al. (2018) for major elements, and Lightfoot et al. (1993) for Co.

Table 3. Modeled results for the evolution of Co concentration in the residual komatiitic and basaltic magmas and their crystal cumulates during fractional crystallization.

T, °C	MgO melt, wt.%	Mass of Ol, g	Mass of CPx, g	D_{Co} ol/melt	D_{Co} cpx /melt	% of crystal-lization	Co content in melt, ppm	Cumulative Co content in crystal cumulate, ppm	Melt %
Komatiite									
1600	27.0	-	-	1.31	0.46	0	104	0	100
1550	26.6	1.6	-	1.33	0.46	2	103	138	99
1500	23.5	11.1	-	1.49	0.50	13	97	150	88
1450	20.6	8.7	-	1.67	0.55	21	92	147	79
1400	17.9	6.9	-	1.90	0.61	28	87	144	73
1350	15.4	5.6	-	2.18	0.67	34	83	143	67
1300	13.1	4.7	-	2.53	0.75	39	78	143	62
1250	10.9	3.9	-	2.96	0.85	43	74	143	58
1200	9.0	3.3	-	3.51	0.96	46	69	144	55
1150	7.4	2.9	-	4.23	1.11	49	65	145	52
Basalt									
1200	7.4	-	-	4.21	1.10	0	44	0	100
1150	5.9	7.2	-	5.16	1.29	21	37	227	79
1100	3.8	5.5	7.6	7.75	1.75	48	23	157	52
1050	1.9	2.2	5.3	14.36	2.79	63	12	135	37
1000	0.8	1.6	2.1	29.69	4.83	71	3	131	29
950	0.4	1.1	1.1	63.60	8.58	76	0.2	129	24
900	0.1	0.6	0.5	173.10	18.28	79	0.0	127	21

Table 4. The Co concentration and calculated R and N factors for komatiitic and basaltic magmas

	X_i^{sil}	D_i^{sul}	R/N	Y_i^{sul} (Co, ppm)[1]
Komatiittic magma	104	83	1	206/206
	104	83	10	1,021/1,072
	104	83	50	3,310/3,963
	104	83	100	4,764/6,076
	104	83	1000	7,978/8,632
	104	83	10000	8,562/8,632
Basaltic magma	44	68	1	87/87
	44	68	10	422/447
	44	68	50	1,293/1,579
	44	68	100	1,799/2,315
	44	68	1000	2,804/2,992
	44	68	10000	2,972/2,992

[1] The Co concentrations assuming R and N factors (R/N)

Table 5 Thermodynamic data for cobalt minerals

Name	Cobalt	Cobalt monoxide	Tricobalt tetroxide	$Co(OH)_2$	Cattierite	Linnaeite	Cobaltpentlandite
Formula	Co	CoO	Co_3O_4	$Co(OH)_2$	CoS_2	Co_3S_4	Co^9S_8
Reference	RH	RH	RH	BR	PZ	PZ	PZ
G, J	0	-214,100	-802,200	-569,229	-147,365	-346,347	-816,330**
S, J	30.04	52.83	109.3	93.303	74.793	175.937	410.752***
V, cm^3*	6.67	11.64	39.77		25.52	62.12	149.33
a1.a		-30.47	132	82.8	65.8	153	3.95E+01***
a2.b	0.0418	0.0295	0.066	47.7	0.0303	0.0825	2.71E-02***
a3.c	-156,000	-4,170,000	-2,480,000		-587,000	-1,340,000	-3.79E+05***
a4.d	269	1,930					
c1.e	-0.0000165						

RH - Robie and Hemingway (1995)
BR - Barin et al. (1977)
PZ - Pankratz et al. (1987)
* Calculated from the relationship $Vm=N_{avogadro}*V_{cell}/Z$ (number of formula units in the unit cell; Z and V_{cell} are from mindat.com
** Calculated from the relationship $\Delta G=\Delta H-T\Delta S$, for $CoS_{0.89}$*9, ΔH=22,600 Cal (see Mills, 1974, Stuve et al., 1985)
*** From (Pankratz et al., 1987) multiplied by 9

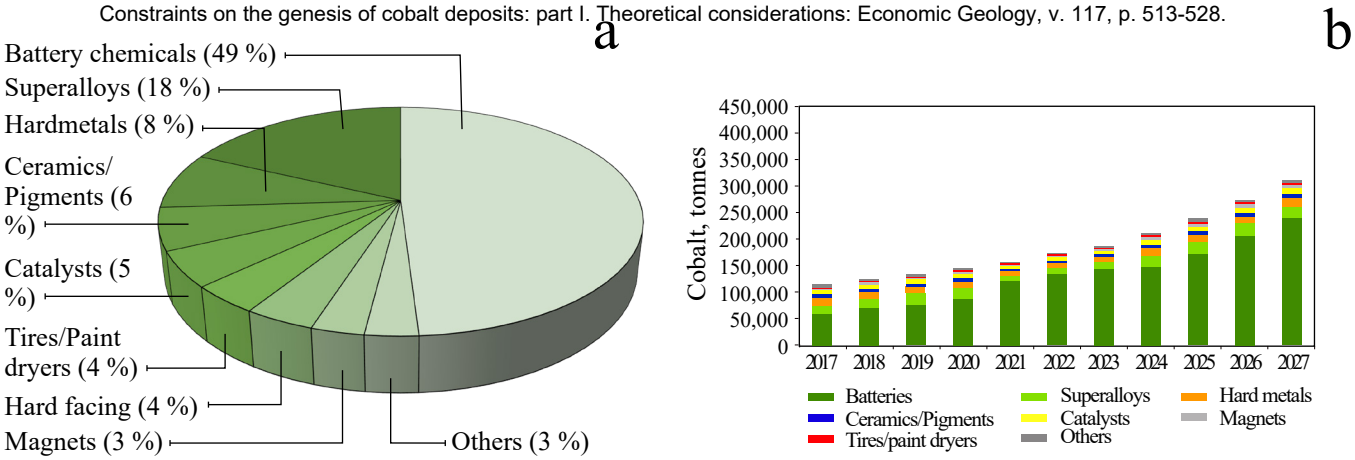

Figure 1 a) The main uses of cobalt; b) Current and predicted future demand for cobalt as a function of use. Modified from Alves Dias et al. (2018).

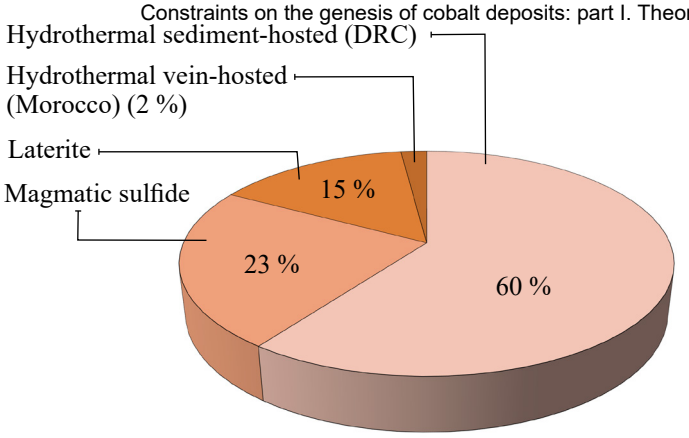

Figure 2 Cobalt resources as a function of deposit type. Modified from Slack (2017).

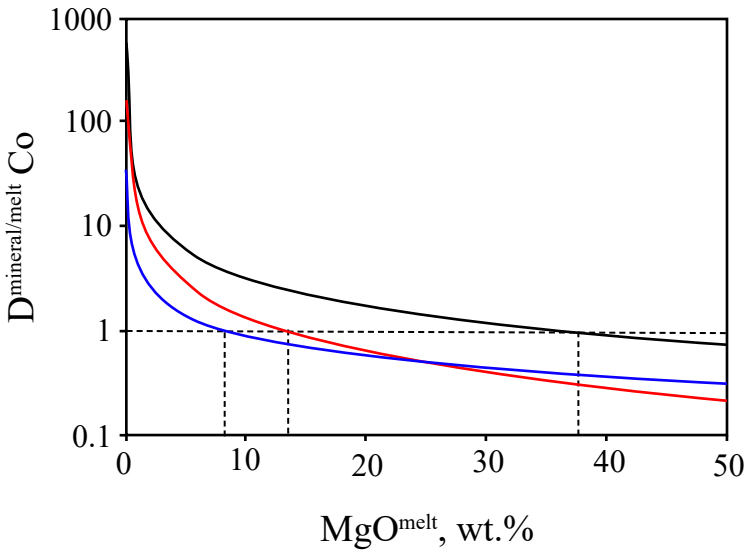

Figure 3 Cobalt mineral-melt partition coefficients for olivine (black), orthopyroxene (red) and clinopyroxene (blue) as a function of the MgO content of the magma. The horizontal dashed line indicates equal partitioning of cobalt into mineral and melt. The intersections of this line with the partition coefficient curves for the minerals indicate the MgO content of the magma, below which Co prefers the mineral (vertical dashed lines). The partition coefficients were calculated from the data of Bedard (2005, 2007 and 2014).

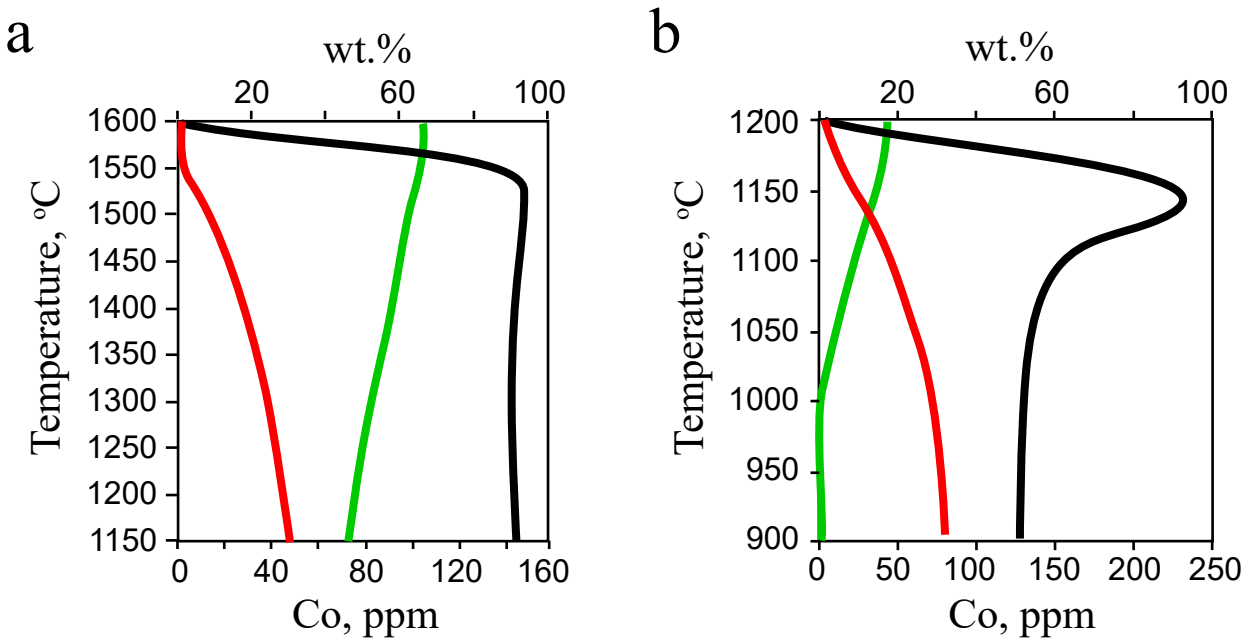

Figure 4 The modeled Co content of the magma (green), the percent magma crystallized (red) and the Co content of the crystal cumulate (black) with decreasing temperature during the fractional crystallization of: a) a komatiitic magma and b) a basaltic magma. This modeling was carried out using the computer program, Pele (Boudreau, 1999). See main text for further explanation.

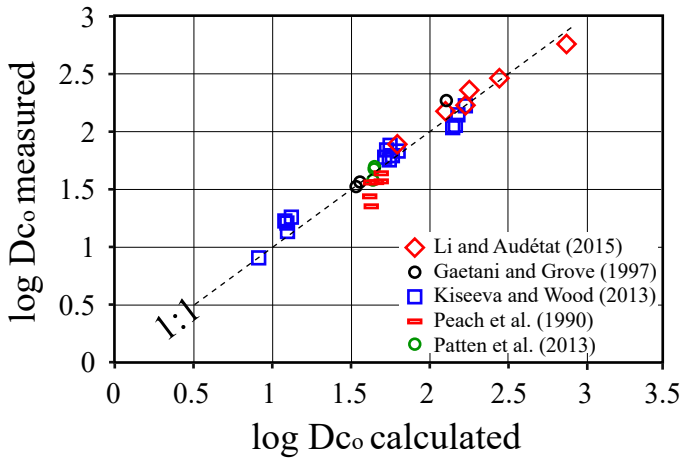

Figure 5 A comparison of measured Co sulfide-silicate partition coefficients to those predicted using Equation (5) in Li and Audétat (2015).

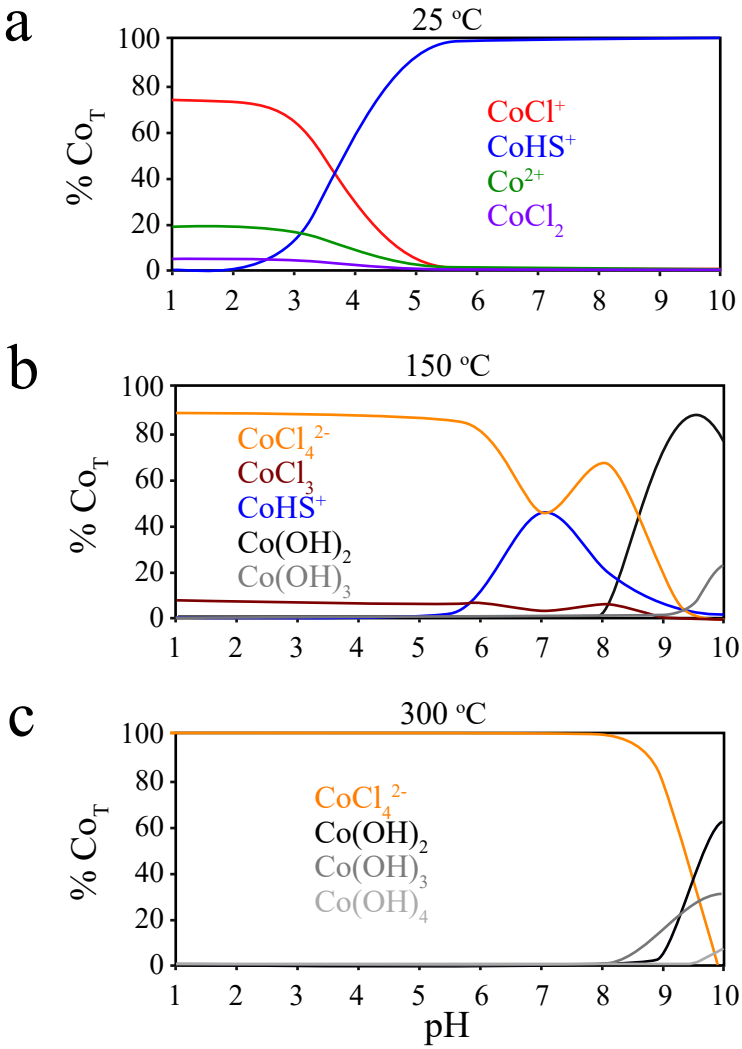

Figure 6 The aqueous speciation of Co as a function of pH for a fluid with a Cl- activity of 1, a H2S activity of 0.001 and a Co concentration of 0.01 M at: a) 25 °C, b 150 °C and c) 300 °C. The thermodynamic data for Co2+ were taken from Shock et al. (1997), the data for the hydroxide species from Pyasunova et al. (1998) and the chloride and bisulfide species from Migdisov et al. (2011).

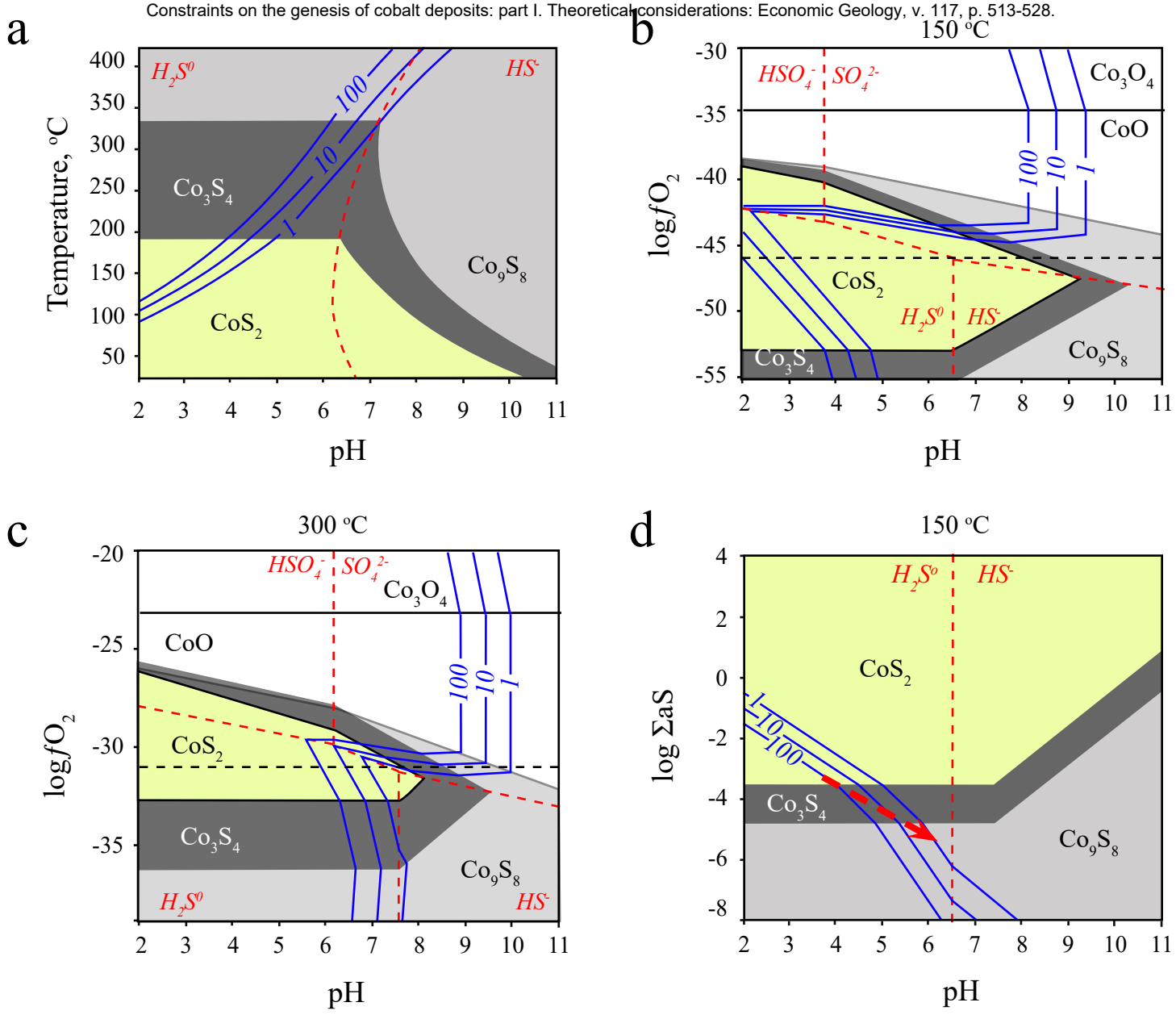

Figure 7 Stability relationships for the Co minerals, cattierite (CoS2), linnaeite (Co3S4), cobaltpentlandite (Co9S8) and guite (Co3O4) and the solid, CoO, as a function of a) temperature and pH, b) log fO2 and pH at 150 °C, c) log fO2 and pH at 300 °C, and d) log ΣaS and pH at 150 °C. Also shown are the predominance boundaries for aqueous sulfur species and solubility contours for the cobalt minerals assuming that Co was dissolved as the species CoCl42-. The thermodynamic data for the minerals shown in these diagrams are reported in Table 5 and the thermodynamic data for CoCl42- were taken from Migdisov et al. (2012). All other thermodynamic data were taken from the database in the HCh software package (Shvarov, 1999). The horizontal black dashed line in (b) and (c) is the MH buffer.

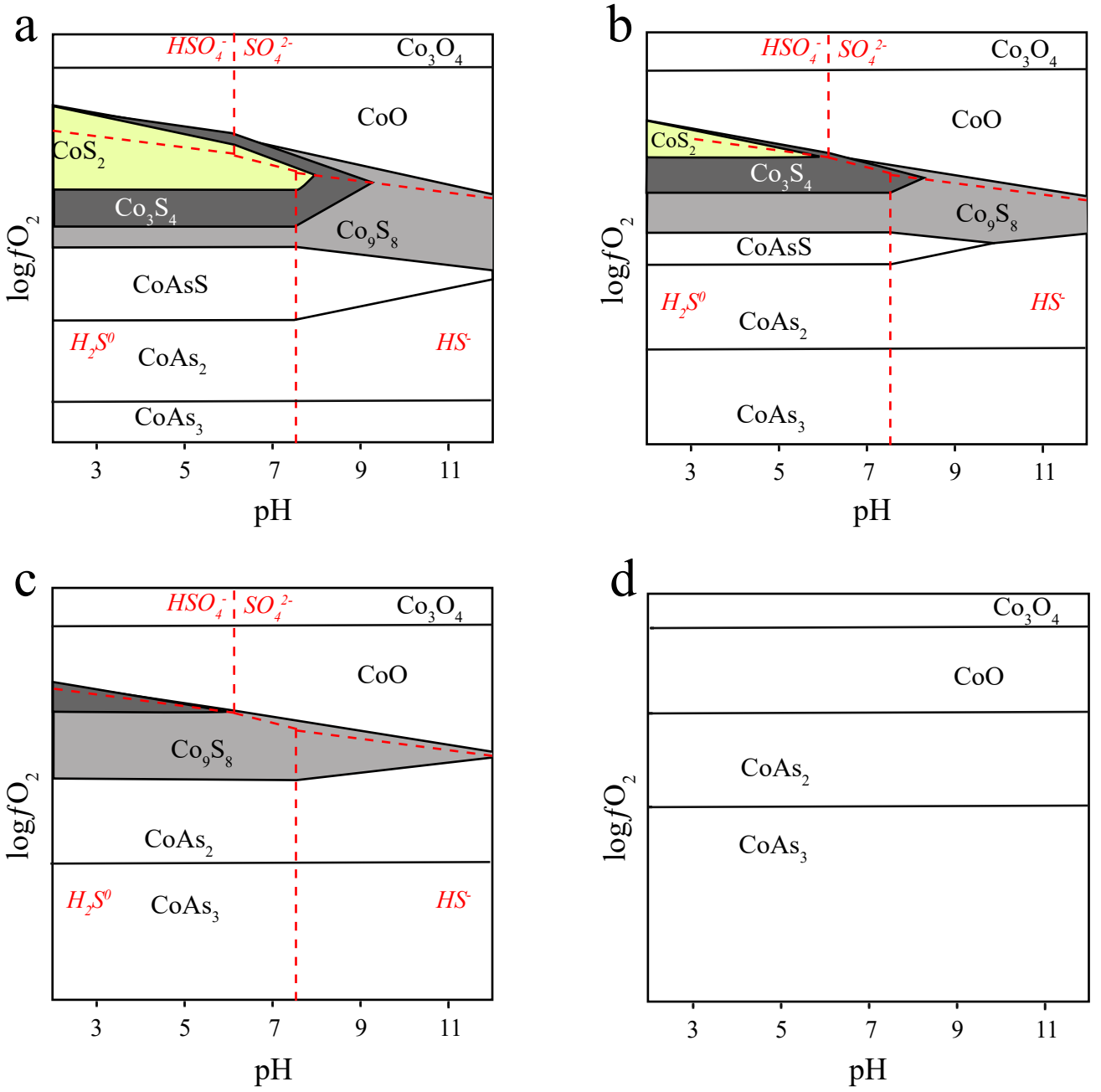

Figure 8 Diagrams showing the stability relationships of the sulfide and oxide minerals/phase considered in Figure 7, the sulfaresenide, cobaltite (CoAs), and the arsenides, safflorite (CoAs2) and skutterudite (CoAs3) as a function of *f*O2 and pH. They were constructed using chemographic analysis, in which the slopes of the stability boundaries were determined by the Gibbs Duhem equation and their relative locations were dictated by the direction of redox and pH changes across these boundaries. This construction assumed that the dissolved sulfur species are H2S, HS-, HSO4- and SO42- and As is present as the species H3AsO30. The diagrams are ordered from a) to d) to reflect a progressive increase in the activity of As and a corresponding decrease in the activity of S.

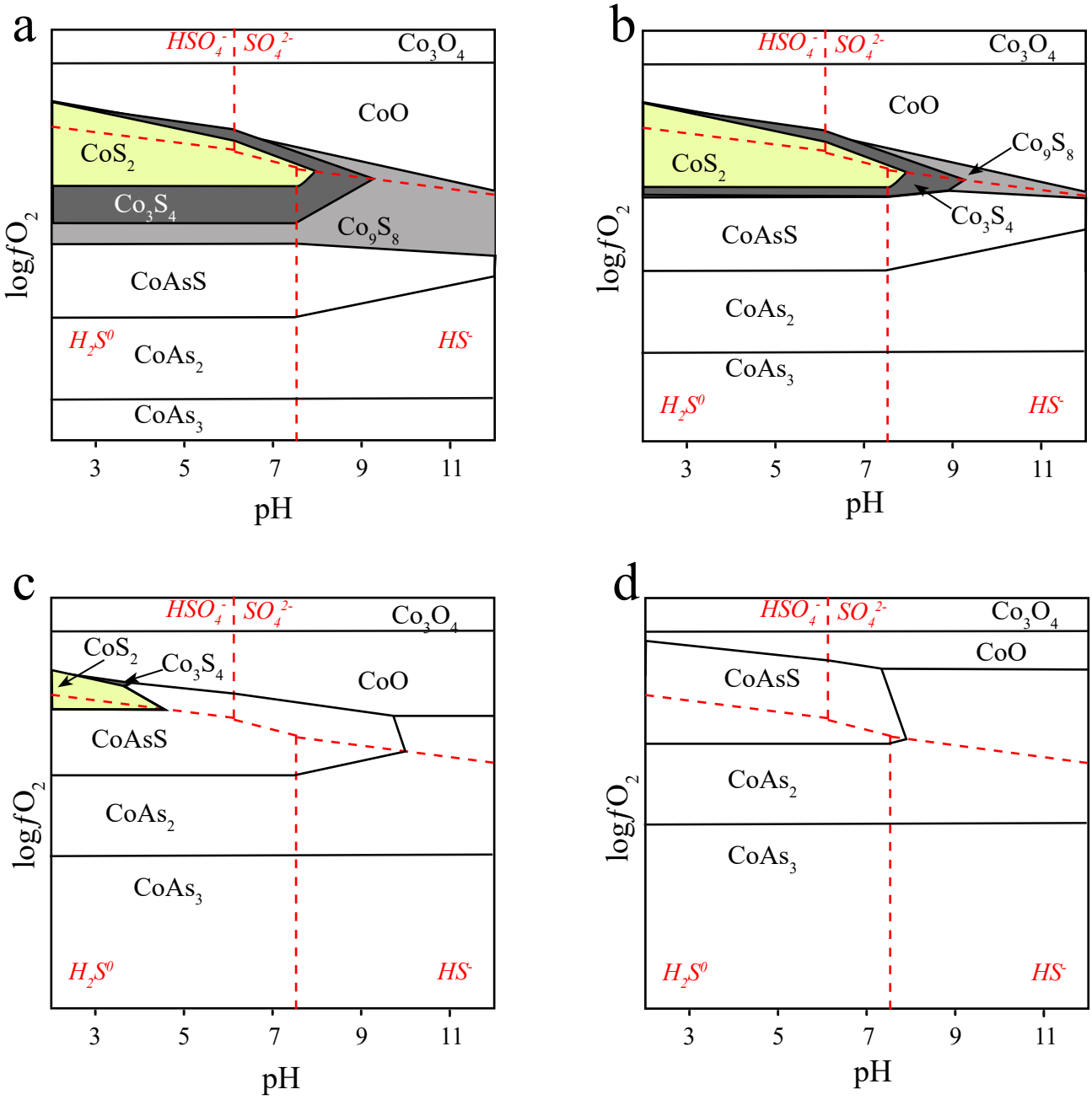

Figure 9 Stability relationships as a function of *f*O2 and pH for the phases considered in Figure 8. They are ordered from a) to d) to reflect a progressive increase in the activity of As at constant activity of S.